ARTICLES
https://doi.org/10.1038/s41589-021-00791-w

nature chemical biology

Check for updates

A molecular trap inside microtubules probes luminal access by soluble proteins

Yuta Nihongaki ✉, Hideaki T. Matsubayashi and Takanari Inoue ✉

The uniquely hollow structure of microtubules (MTs) confers characteristic mechanical and biological properties. Although most regulatory processes take place at the outer surface, molecular events inside MTs, such as α-tubulin acetylation, also play a critical role. However, how regulatory proteins reach the site of action remains obscure. To assess luminal accessibility, we first identified luminally positioned residues of β-tubulin that can be fused to a protein of interest. We then developed a chemically inducible technique with which cytosolic proteins can be rapidly trapped at the lumen of intact MTs in cells. A luminal trapping assay revealed that soluble proteins of moderate size can enter the lumen via diffusion through openings at the MT ends and sides. Additionally, proteins forming a complex with tubulins can be incorporated to the lumen through the plus ends. Our approach may not only illuminate this understudied territory, but may also help understand its roles in MT-mediated functions.

Microtubules (MTs) are dynamic cytoskeletal elements that are crucial for a wide variety of cellular functions including cell division, cell migration, neuronal plasticity and ciliogenesis. Composed of polymerized α- and β-tubulin subunits, MTs form hollow tubes ~14 nm in inner diameter, and are regulated by diverse factors such as MT-associated proteins (MAPs) or post-translational modifications (PTMs)[1–3] to enable multifaceted roles. Whereas many processes regulating MT dynamics take place on the surface or ends of MTs, molecular processes that occur in the lumen of MTs are much less known.

Explorations of molecular events inside MTs have led to several important findings. Electron microscopy studies found electron-dense particles in the lumen of cellular MTs of various organisms[4–6]. Although the molecular identity and biological significance of these particles remain elusive, these observations imply that biomolecules can enter the MT lumen and modulate the stability and function of MTs from the inside. Recent studies have revealed that the well-known α-tubulin K40 acetylation[7], located in the MT lumen, affects MT mechanical resilience, cell signaling and cell migration[8–11]. The widely conserved protein most responsible for acetylating K40, α-tubulin acetyltransferase 1 (αTAT1)[12,13], is believed to enter the MT lumen before catalysis. This is because K40 acetylation is observed only in tubulin dimers that are assembled into polymerized MTs, and not those existing as a free dimer in the cytosol[13]. Collectively, these studies indicate that proteins can access the MT lumen and conduct biochemical reactions to regulate the mechanical and biological properties of MTs.

This raises a fundamental question of how proteins can gain access to the MT lumen, an environment surrounded by a cylindrical wall of densely packed tubulin dimers. There are several potential mechanisms for protein entry into the inside of MTs: incorporation at polymerizing MT plus ends via binding of protofilaments or free tubulin dimers, or diffusion through MT ends or lateral defects[14] (Fig. 1a). Many in vitro studies using purified MTs have shown that a protein as large as 160 kDa can access the lumen of purified MTs[15–18]. More specifically, in unfixed conditions, purified in vitro MTs can be stained with monoclonal antibody 6-11B-1 against luminal acetylated K40 of α-tubulin[17]. Another study also showed that rabbit polyclonal antibody against K40 acetylation can access the lumen of unfixed in vitro MTs[18]. Because purified MTs in these experimental conditions were stabilized (that is, little to no polymerization), the observed luminal access is probably by diffusion through MT open ends and sides such as lateral defects. Theoretical modeling, by contrast, suggests that a molecule that binds to the MT lumen at high affinity would require a long time (such as years for antibodies) to reach equilibrium if allowed diffusive entry solely at MT ends[19], contrasting to the efficient luminal entry observed in MTs prepared in vitro. Although electron microscopy and atomic force microscopy have shown lateral defects and side cracks in MTs[16,20–23], the widely used MT stabilizing agent taxol is reported to affect the ultrastructure of MTs[21]. In addition, purified MTs exhibit unexpected permeability, probably due to their non-physiological assembly state[17]. Moreover, unlike purified MTs, the surface and luminal parts of MTs in cells are decorated by various MAPs[2]. Taken together, whether and how intact MTs in living cells grant luminal accessibility to soluble proteins remain not fully understood, and a technique to directly probe protein accessibility to the MT lumen in cells is lacking.

To overcome the challenge, we set out to develop a chemically inducible technique with which soluble protein probes can be rapidly trapped at the lumen of intact MTs in living cells. Combined with pharmacological perturbations, the luminal trapping assay revealed two entry mechanisms of soluble proteins: diffusion through openings at the MT ends and sides, and incorporation, along with tubulins, into the MT plus ends.

Results

Screening luminal tubulin residues for protein anchoring. To quantitatively visualize the accessibility of proteins into the lumen of MTs in living cells, we devised a molecular strategy where chemically inducible dimerization (CID)[24] was adapted to achieve rapidly inducible trapping of cytosolic proteins at the MT lumen (Fig. 1b). One of the most prevalent CIDs relies on a pair of proteins: FK506-binding protein-12 (FKBP) and FK506-rapamycin-binding domain (FRB), which heterodimerize in a rapamycin-dependent manner. The CID scheme enables guided subcellular translocation

Department of Cell Biology and Center for Cell Dynamics, Johns Hopkins University School of Medicine, Baltimore, MD, USA.
✉e-mail: ynihong1@jhmi.edu; jctinoue@jhmi.edu

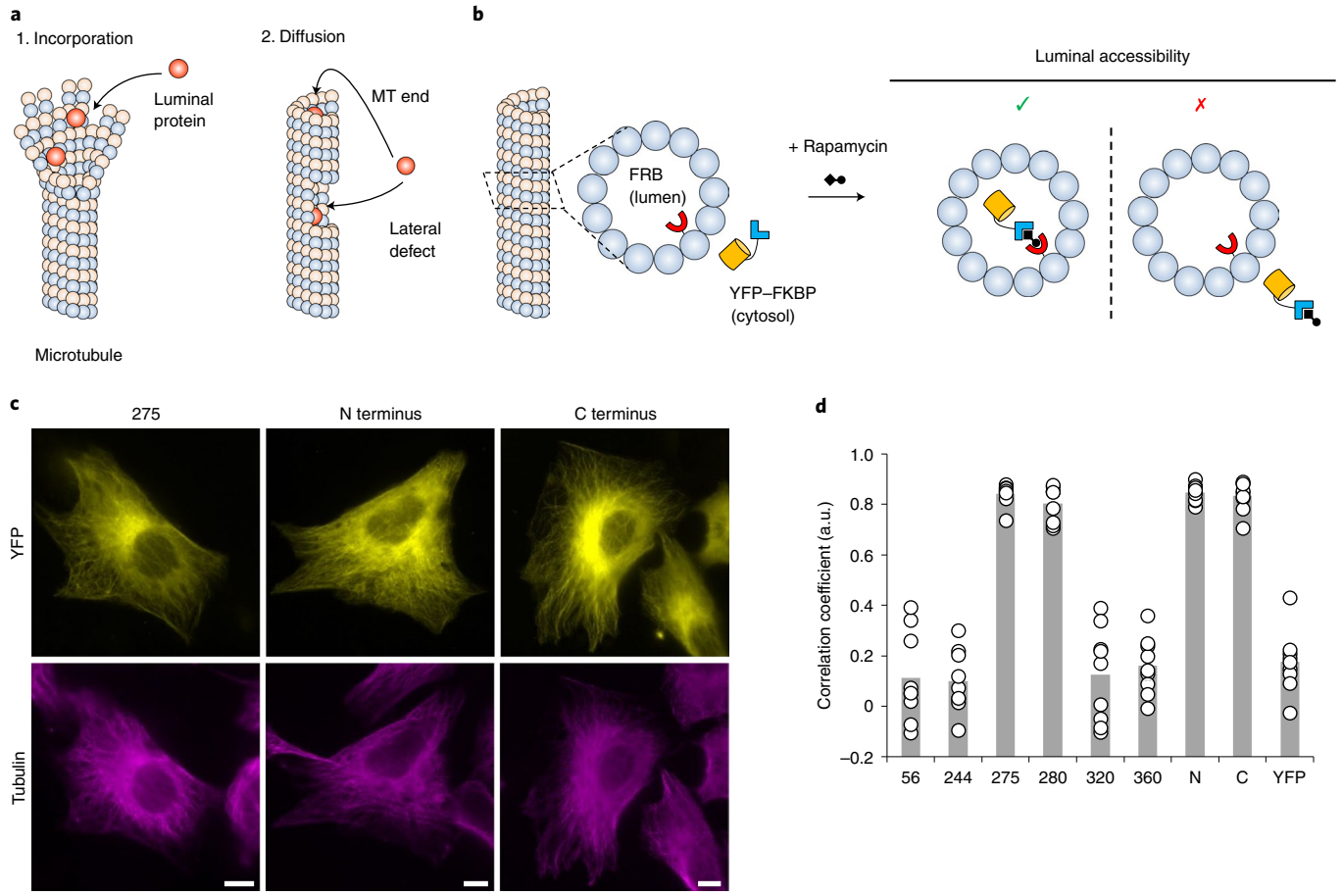

Fig. 1 | Anchoring a protein of interest inside MTs to develop a chemically inducible luminal protein trap system. a, Possible mechanisms of protein entry into the lumen of MTs: (1) incorporation of luminal proteins at the plus end of growing MTs via interaction with protofilaments and cytosolic tubulin dimers or (2) diffusion from the open extremities or lateral defects of MTs. **b**, Schematic of the chemically inducible intraluminal protein trap system. It consists of two fusion proteins—YFP–FKBP and FRB—anchored inside MTs. If YFP–FKBP in the cytoplasm can access the inside of MTs, the YFP–FKBP can be trapped to FRB anchored to the lumen of MTs by rapamycin treatment. This process can be visualized in living cells by fluorescence microscopy as translocation of the YFP signal. **c**, Localization of YFP-inserted β-tubulin. The YFP insertion sites are indicated at the top. U2OS cells transfected with YFP-fused tubulins (yellow) were immunostained for total tubulin (magenta). Scale bars, 10 μm. **d**, Quantification of colocalization between YFP-inserted tubulins and MTs. The degree of MT localization was determined by the Pearson's correlation coefficient between YFP and total tubulin. The YFP fusion sites are indicated. The YFP–tubulin constructs showing no fluorescence (79, 84 and 356) are not quantified. Dots are individual data points and bars indicate means ($n = 9$ from three individual experiments).

of a protein of interest, providing a powerful means for manipulating cellular signaling and probing the dynamics of proteins[24,25]. Here, we envisioned that an FRB protein engineered to be anchored to the MT lumen should be able to trap a cytosolic FKBP fusion protein following an experimental trigger, namely adding rapamycin. Time-lapse fluorescence imaging of protein accumulation can then allow us to visualize the kinetics and extent of protein accessibility into the lumen of MTs, in real time, for quantitative assessment.

One way to anchor FRB to the MT lumen is to directly fuse FRB to tubulin amino-acid residues that face the MT lumen, making sure that the resulting fusion protein does not cause abnormal MT organization. In the high-resolution cryo-EM structure of MTs[26], several loop structures as well as the N terminus of β-tubulin are exposed to the lumen, whereas its C terminus faces the cytosol (Extended Data Fig. 1a). We thus tested nine amino-acid residues within these loops, along with the N terminus, as potential insertion sites (Extended Data Fig. 1b). We first constructed 11 YFP-fused β-tubulins (nine internal insertions and one N terminus fusion, along with one C terminus as a control), and expressed each of them in human U2OS cells (Fig. 1c and Extended Data Fig. 1c). Some of the fusion proteins did not express at a detectable level in our experiment (79, 84 and 356). For those expressed, we quantified Pearson's correlation coefficient to determine the extent of colocalization between each YFP fusion and the total MTs stained with a tubulin antibody[27], and found that fusion proteins at residue 275 and 280 as well as the N and C termini localized to MTs without altering the apparent MT organization (Fig. 1d). As residues 275 and 280 are located within the same loop, we pursued residue 275 for the following characterizations.

Monoclonal antibodies against luminal MT epitopes gain access to the inside of cellular MTs only after standard fixation[17,28,29]. Based on antibody staining with and without fixation, we next confirmed the luminal topology of FRB at the two promising fusion sites, namely 275 and the N terminus, expecting that FRB–β-tubulin (Tub-FRB$_{lumen}$) and β-tubulin$_{1–275}$–FRB–β-tubulin$_{276–444}$ (Tub-FRB$_{lumen\text{-}ins}$) position the FRB in the lumen side of MTs (Fig. 2a,b), whereas a control β-tubulin–FRB (Tub-FRB$_{outer}$) is located at the outer surface of the MTs. For antibody detection of FRB-fused tubulin, a V5 tag was introduced adjacent to FRB. In V5 antibody staining following fixation, all Tub-FRB$_{lumen}$, Tub-FRB$_{lumen\text{-}ins}$ and Tub-FRB$_{outer}$ showed MT

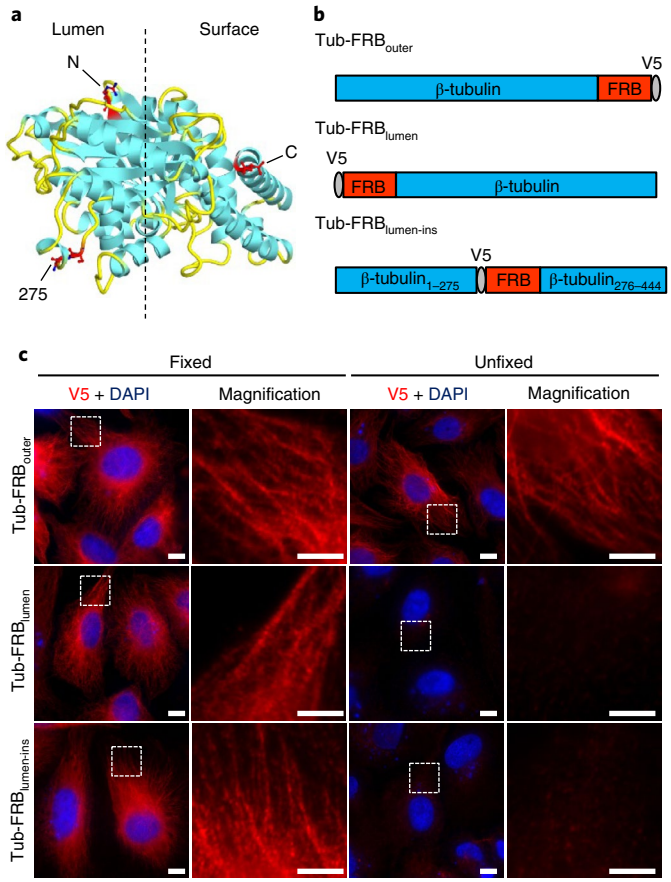

Fig. 2 | Generation and validation of FRB-fused β-tubulins. a, FRB fusion sites in β-tubulin. The N terminus and Ser275 are positioned to the inside of the MTs, and the C terminus is on the outer surface of the MTs. The fusion sites are highlighted in red. The loop region in the structure is colored in yellow, otherwise in cyan (PDB 3J6G). **b**, Constructs of FRB-fused tubulins. Although Tub-FRB$_{outer}$ localizes its FRB to the outer surface of the MTs, the FRBs of Tub-FRB$_{lumen}$ and Tub-FRB$_{lumen-ins}$ localize to the lumen of the MTs. The V5 tag adjacent to FRB is used for the immunofluorescence. **c**, Immunofluorescence of fixed U2OS cells (left) and unfixed cellular MTs (right) expressing FRB-fused tubulins. The samples were stained with V5 antibody (red) and DAPI (blue). Transduced FRB-fused tubulins are indicated. Representative images from three individual experiments are shown. Magnified images of the regions outlined by white squares are also shown. Scale bars, 10 μm.

patterns (Fig. 2c and Extended Data Fig. 1d,e), confirming their MT localization. Next, we performed V5 antibody staining with no fixative, and observed that while Tub-FRB$_{outer}$ was detected by V5 antibody, Tub-FRB$_{lumen}$ and Tub-FRB$_{lumen-ins}$ were not. This result supports that the FRB proteins of Tub-FRB$_{lumen}$ and Tub-FRB$_{lumen-ins}$ are located inside MTs.

Microtubule luminal accessibility tested in living cells. To test how efficiently these luminal FRB-fused tubulins can trap FKBP upon rapamycin treatment, we generated U2OS cells stably expressing Tub-FRB$_{outer}$, Tub-FRB$_{lumen}$ and Tub-FRB$_{lumen-ins}$, respectively, and transduced these cells with YFP–FKBP and a live-cell fluorescence marker for MTs, a CFP fusion with the MT-binding domain of MAP4 (CFP–MAP4m)[30]. In all three FRB-fused tubulins tested, we observed YFP–FKBP translocation to MTs from the cytosol within 10 min of rapamycin treatment (Fig. 3 and Supplementary Videos 1–3), albeit with different kinetics. Although Tub-FRB$_{outer}$ showed rapid translocation of YFP–FKBP ($t_{1/2}$ (half-time for YFP-FKBP accumulation at MTs) < 1 min), Tub-FRB$_{lumen}$ and Tub-FRB$_{lumen-ins}$, which anchor FRB to the inside of the MTs, exhibited slower translocation ($t_{1/2}$ = 7.2 min and 5.5 min, respectively). The observed slower translocation with the luminal FRBs implies that, although the lumen of MTs are accessible from the cytoplasm, this accessibility is limited compared to the outer surface. Of note, we observed little to no noticeable effect on the organization or dynamics of the MTs during the trapping assays.

Luminal protein incorporation into growing MTs. To visualize the YFP–FKBP translocation with higher spatiotemporal resolution, we repeated the assay with total internal reflection fluorescence microscopy (TIRF), intending to capture molecular events taking place at individual MTs (Extended Data Fig. 2 and Supplementary Videos 4–6). When the outer surface FRB (Tub-FRB$_{outer}$) was used for trapping, accumulation of YFP–FKBP fluorescence was observed uniformly along the single MTs after rapamycin treatment (Extended Data Fig. 2a,b, top). By contrast, when a luminal FRB such as Tub-FRB$_{lumen}$ or Tub-FRB$_{lumen-ins}$ was used, YFP translocation was initially observed only at the extremities of the MTs, then gradually propagated along the entire MTs over the next several minutes (Extended Data Fig. 2a,b, middle and bottom). We then confirmed that most MT ends at the cell periphery are EB1-positive and hence plus ends (Extended Data Fig. 3).

As illustrated in Fig. 1a, there are two plausible routes for the observed luminal entry. First, YFP–FKBP can be incorporated into the growing MT ends through binding to Tub-FRB within protofilaments or free tubulin dimers, and then gradually shift its relative localization toward the middle part of the MTs as they continuously grow. Second, YFP–FKBP can diffuse into the lumen from openings at the edges and sides of the MTs. These two mechanisms are expected to be non-mutually exclusive. To understand if and how well each of these mechanisms takes place, we first assessed the incorporation by performing a luminal trapping assay in the presence of nocodazole. Nocodazole halts MT polymerization and dissolves short-lived dynamic MTs[8], while residual MTs remain stable for several hours without exhibiting any further polymerization. Performing the trapping assay in these residual static MTs thus allows us to exclude the contribution from incorporation into the MT plus ends. We first confirmed that MT polymerization ceased within 1 min of nocodazole treatment at 5 μM, as indicated by the rapid disappearance of the MT polymerization marker EB1–mCherry from the MTs that were marked by CFP–MAP4m (Extended Data Fig. 4 and Supplementary Video 7). Based on this observation, we decided to treat cells with nocodazole for 20 min before initiating the luminal MT trapping assays. In cells expressing Tub-FRB$_{outer}$, YFP–FKBP translocated to the MTs upon rapamycin treatment (Extended Data Fig. 2c, top and Supplementary Video 8). By contrast, when FRB is positioned to the inside of MTs using Tub-FRB$_{lumen}$ or Tub-FRB$_{lumen-ins}$, translocation of YFP–FKBP was not detected (Extended Data Fig. 2c, middle and bottom, and Supplementary Videos 9 and 10), even after permeabilization of plasma membranes for the removal of YFP–FKBP in the cytosol (Extended Data Fig. 5). We also repeated the same trapping experiment followed by identification of stable MTs using an antibody against acetylated tubulins that can distinguish stable MTs from dynamically polymerizing ones. Fluorescence images and line-scan analysis thereof detected colocalization between YFP–FKBP and stable MTs in cells with the MT surface trap, but not with the luminal traps (Extended Data Fig. 6a), regardless of the presence of nocodazole (Extended Data Fig. 6b). To make sure that the observed inability of YFP–FKBP to access the lumen in the presence of nocodazole was not due to severely altered MT organization from the drug treatment, we washed out the nocodazole after rapamycin treatment in the trapping assay, and we could detect a

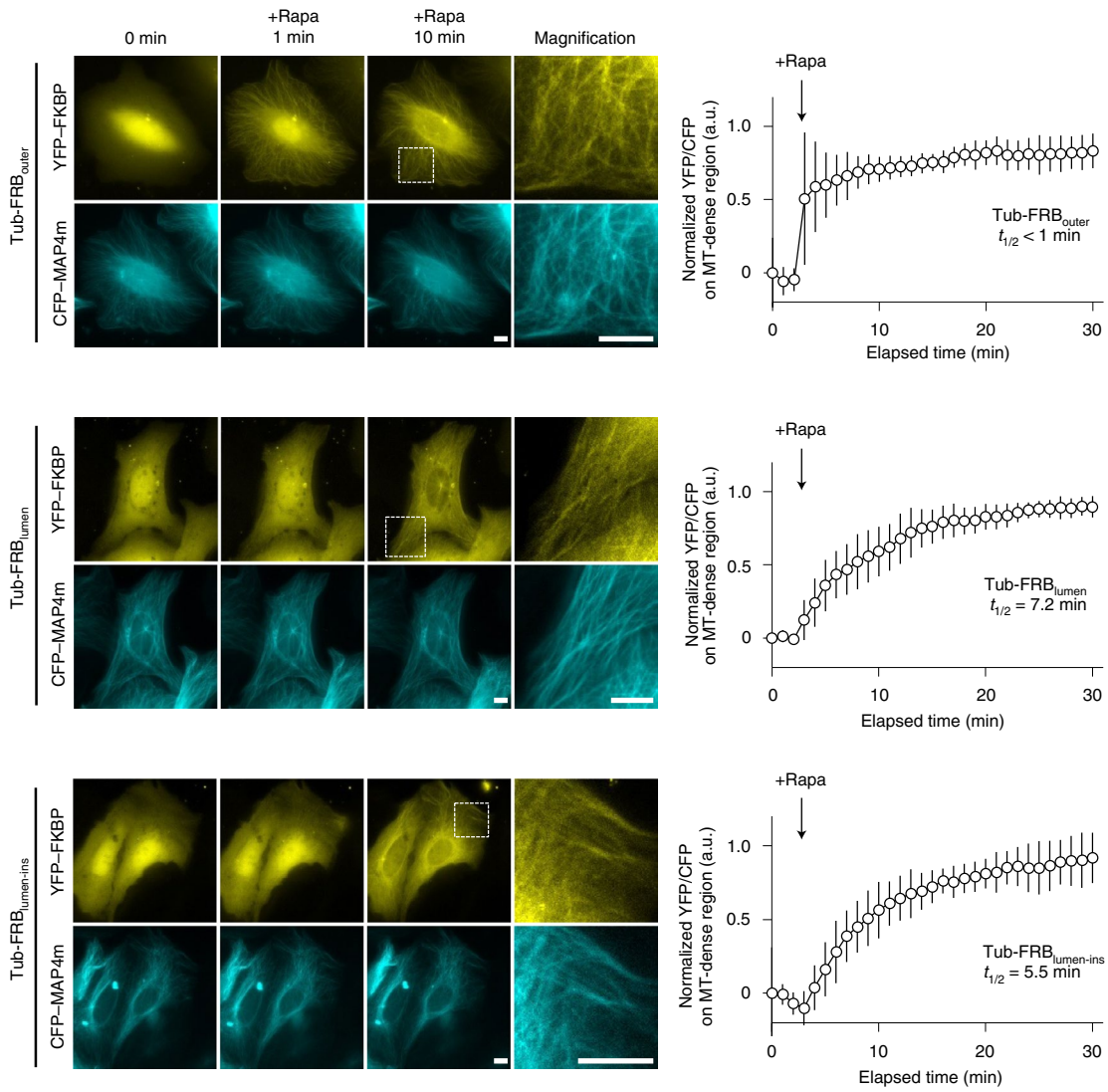

Fig. 3 | An inducible luminal trap reveals limited accessibility to the lumen of MTs. Left: translocation of YFP–FKBP in U2OS cells stably expressing FRB-fused tubulins. The indicated FRB-fused tubulins were expressed. CFP–MAP4m was also co-transduced for visualizing the MTs. Magnified images of the regions outlined by white squares 10 min post rapamycin treatment are also shown. Rapa, 100 nM rapamycin. Right: quantification of the YFP–FKBP translocation kinetics in the left panels. To quantify the signal on MTs without including the signal from cytoplasm in the wide-field fluorescence imaging, we manually selected regions of interest at MT dense regions. The normalized average YFP/CFP ratio from each region is presented as mean ± s.d. (n = 12 cells from three individual experiments). For each region in the cell, the maximal YFP/CFP is normalized to 1 and the initial YFP/CFP is normalized to 0. The half-time of translocation is also shown. Scale bars, 10 μm.

recovered accumulation of YFP–FKBP along MTs expressing the luminal traps (Extended Data Fig. 7).

Taxol is another chemical used for MT stabilization, doing so by binding to the MT lumen. We next examined how taxol impacts luminal accessibility using the trapping assay. In taxol-treated cells, we could observe luminal accumulation of YFP–FKBP, despite the presence of nocodazole (Extended Data Fig. 8). Because nocodazole binds to tubulin dimers, whereas taxol binds to the MTs themselves, it is considered that taxol is less efficient at preserving MT integrity than nocodazole[31]. Consistently, taxol exhibits aberrant MT bundling[32] and induces lattice defects[21]. Therefore, the observed luminal access by YFP–FKBP in taxol-treated cells probably reflects altered MT integrity.

Collectively, these results support that the observed luminal accumulation of YFP–FKBP is primarily driven through its incorporation into the plus ends of polymerizing MTs.

Diffusive luminal entry of soluble proteins. Next, we tested whether soluble proteins enter into the MT lumen by diffusion and travel inside MTs. In the luminal trapping assay described above for stable MTs (Extended Data Fig. 2c), diffusion entry of YFP–FKBP into MTs is precluded for a systemic reason. Nocodazole treatment leads to an increase of free tubulins at the expense of those in complex-forming MTs. Accordingly, the number of FRB-Tub$_{lumen}$ molecules in the cytosol becomes excessive compared to YFP–FKBP molecules. Following the addition of rapamycin, these FRB-Tub$_{lumen}$ molecules in the cytosol could thus exhaust the YFP–FKBP molecules before entering into MTs and binding to the luminal FRB traps. One way to circumvent this is to keep the concentration of YFP–FKBP higher than that of Tub-FRB$_{lumen}$. To achieve this, we made two modifications to the luminal trapping assay: use of a strong promoter (cytomegalovirus, CMV) to drive efficient expression of YFP–FKBP and electroporation to achieve better plasmid

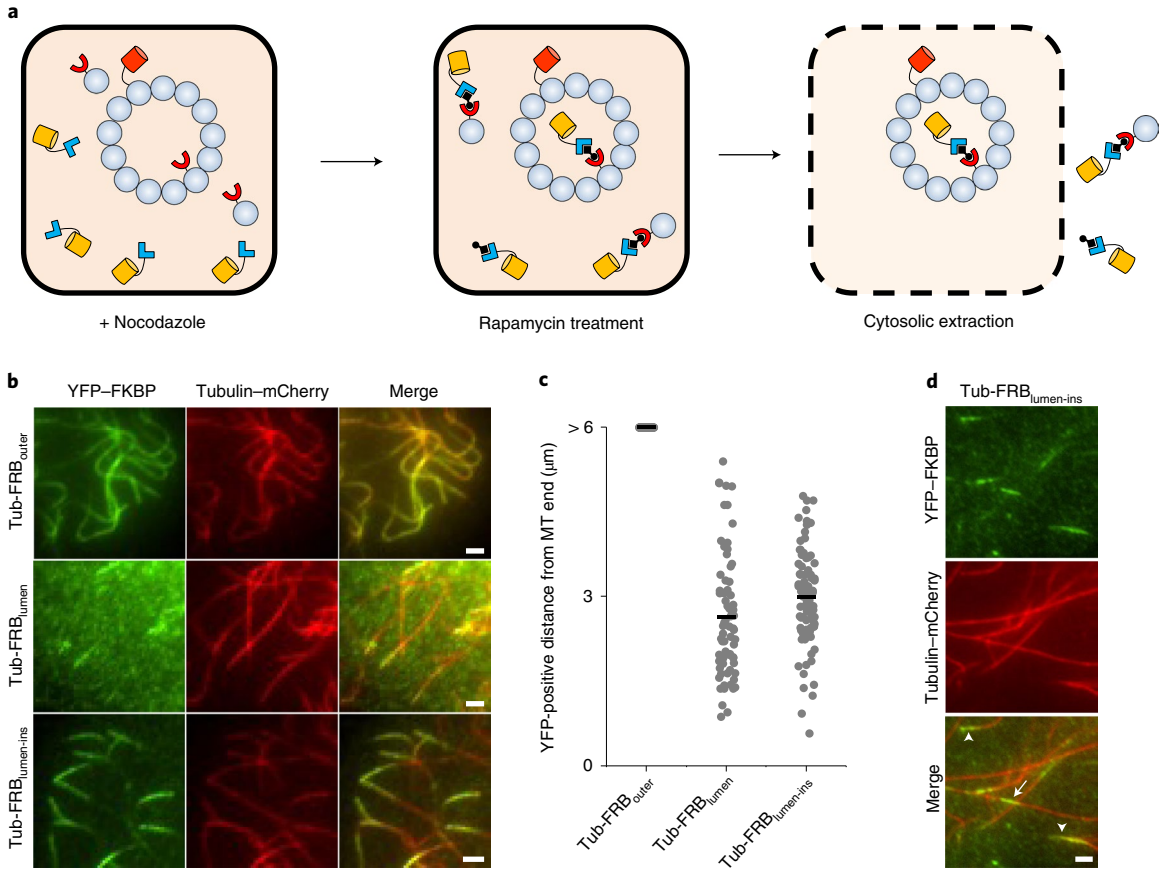

Fig. 4 | Diffusive protein entry into MT lumen in living cells. a, Experimental scheme of the luminal trapping assay for assessing luminal entry via diffusion. U2OS cells expressing Tub-FRB, tubulin–mCherry and YFP–FKBP at high expression levels were treated with nocodazole. The cells were treated with rapamycin for 3 min and subsequently extracted with Triton X-100 to remove cytosolic YFP–FKBP. **b**, TIRF microscopy images from the experiments outlined in **a**. The indicated FRB-fused tubulins were used. Representative images are shown from three individual experiments. Scale bars, 2 μm. **c**, The translocation distance of YFP–FKBP from the MT tips. Gray dots are individual data points. Black horizontal lines indicate the mean ($n = 61$, 72 and 96 cellular MTs, from left to right). **d**, Fluorescence images of luminal translocation at the middle of the MTs from the experiments depicted in **a**. The arrow indicates luminally translocated YFP–FKBP in the middle of the MTs. Arrowheads show YFP–FKBP accumulations at the tips of the MTs. Representative images are shown from three individual experiments. Scale bar, 2 μm.

intake by cells. In addition, cytoplasm extraction was conducted immediately following completion of the luminal trapping to reduce the background signal contributed by the residual YFP–FKBP in the cytosol (Fig. 4a). With this experimental set-up we could observe luminal accumulation of YFP–FKBP, occurring mostly at the tips of the MTs (Fig. 4b,c) and occasionally in the middle part of the MTs (Fig. 4d), suggesting that YFP–FKBP can access the MT lumen via diffusion, probably through open ends and lateral openings.

The observation of diffusive luminal entry then motivated us to directly visualize the process in real time. Toward this end, we made further modifications to the luminal trapping assay and performed luminal trapping using purified YFP–FKBP after cytoplasm extraction (Fig. 5a and Extended Data Fig. 9a). In particular, cells expressing Tub-FRB$_{lumen}$ were extracted by detergent to remove cytosolic Tub-FRB$_{lumen}$, and then subjected to supplementation of a recombinant YFP–FKBP to extracellular media. Subsequent rapamycin addition and fluorescence imaging under a TIRF microscope enabled real-time visualization of YFP–FKBP accumulation at the MT lumen with minimal background signal. Following supplementation of 1 μM YFP–FKBP and rapamycin treatment, YFP–FKBP began to accumulate at the MT tips, then gradually propagated toward the middle part of the MTs (Fig. 5b,c, Extended Data Fig. 9b and Supplementary Videos 11–14). The propagation rate was calculated to be 0.2–0.3 μm min^{-1} (Fig. 5d). The propagation rate became faster (~1 μm min^{-1}) when the YFP–FKBP concentration was increased from 1 to 5 μM (Extended Data Fig. 10a,b). Interestingly, we observed cases where YFP accumulation was initiated at the middle of MTs and propagated bidirectionally along the single MTs (Fig. 5e) at a frequency of 0.059 events per μm (Fig. 5f), suggesting diffusion entry through lateral defects.

Discussion

To investigate MT luminal accessibility in living cells, we have engineered an inducible protein trap inside MTs. Unlike other technologies for detecting protein proximity, such as bimolecular fluorescence complementation[33], the advantage of the inducible trap is to define time point zero by the addition of a chemical inducer, which allows us to quantify the time course of protein entry and perturb cells with a drug such as nocodazole immediately before the experiments. Although previous studies relied on the spatial patterns of acetylated tubulins for the modeling of αTAT1 entry, in this work we visualized the luminal entry process of a model protein in cellular MTs in real time. Our experiment with this luminal protein trapping suggested that a YFP–FKBP protein (35 kDa) can gain access to the lumen of intact MTs in cells through both incorporation (Fig. 3 and Extended Data Fig. 2) and diffusion (Figs. 4 and 5). By contrast, a 160-kDa

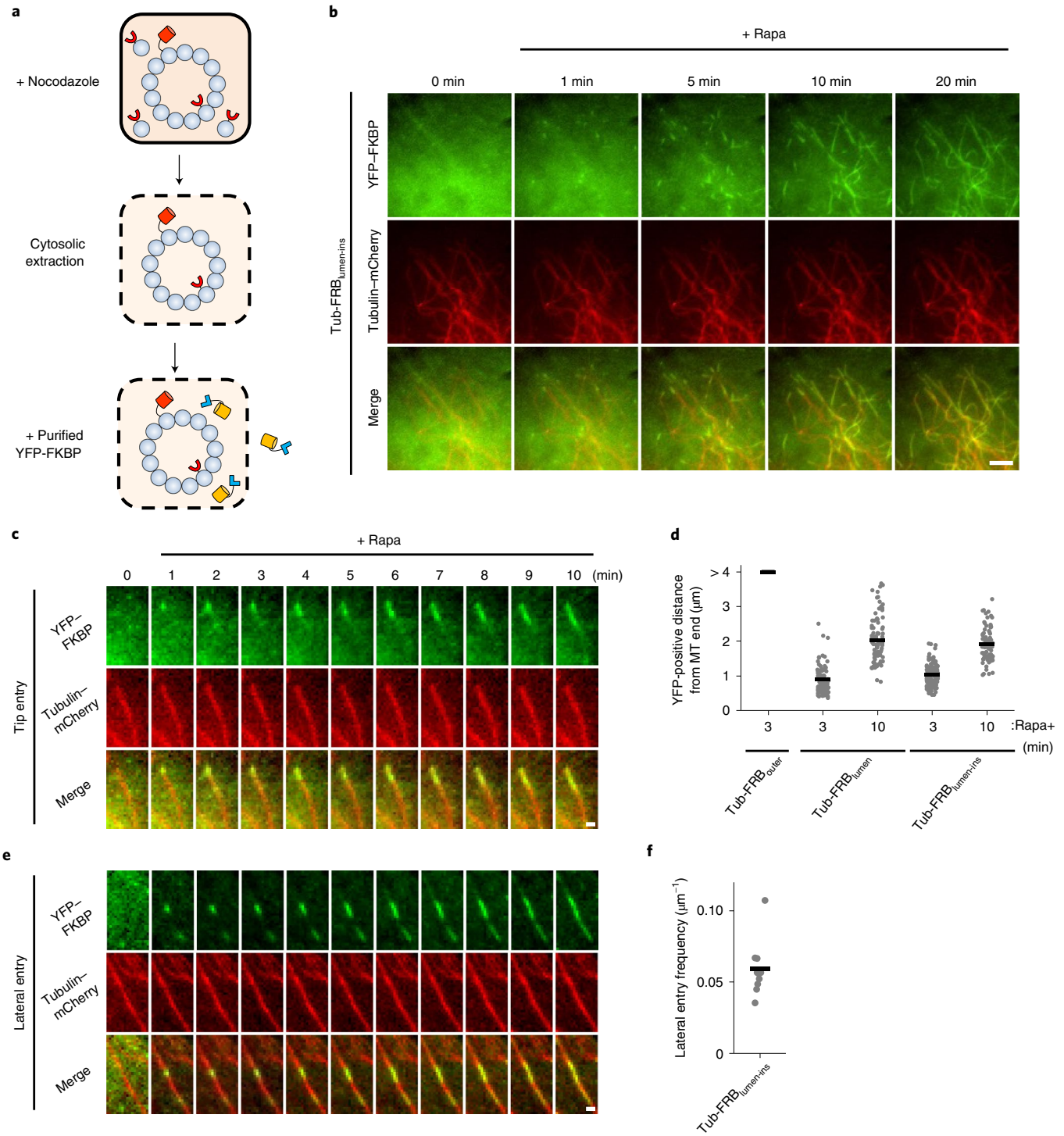

Fig. 5 | Real-time tracking of diffusive protein entry into the MT lumen. a, Experimental scheme of the luminal trapping assay with extracted cellular MTs. U2OS cells expressing Tub-FRB and Tub-mCherry were treated with nocodazole and then extracted with Triton X-100 to remove cytosolic Tub-FRB as free tubulin dimers. The extracted cells were subjected to TIRF imaging with recombinant YFP–FKBP for time-lapse imaging of luminal access by soluble proteins. **b**, Time-lapse TIRF microscopy images from the experiments depicted in **a** with Tub-FRB$_{lumen\text{-}ins}$. Scale bar, 5 μm. Representative images are shown from three individual experiments. **c**, Images of luminal entry of YFP–FKBP from the MT tip with Tub-FRB$_{lumen\text{-}ins}$. Representative images are from three individual experiments. Scale bar, 1 μm. **d**, The translocation distance of YFP–FKBP from the MT tips. The Tub-FRB constructs and rapamycin treatment duration are indicated. Gray dots are individual data points. Black horizontal lines indicate mean (n = 100, 99, 90, 120 and 84 cellular MTs, from left to right). **e**, Images of luminal entry of YFP–FKBP from lateral openings with Tub-FRB$_{lumen\text{-}ins}$. Representative images are from three individual experiments. Scale bar, 1 μm. **f**, Calculated frequency of observed YFP–FKBP lateral entry with Tub-FRB$_{lumen\text{-}ins}$. Gray dots are individual data points from each cell. The black horizontal line indicates the mean (n = 10 cells).

monoclonal antibody targeting the MT lumen cannot reach inside the cellular MTs via diffusion as previously reported (Fig. 2), supporting that the molecular size is one of the determinants of the efficiency of diffusive entry into MTs and traveling inside. So far, two proteins are proposed to function inside MTs in mammalian cells[11,17,34]: αTAT1 (46.8 kDa) and MAP6 (86.5 kDa). Some of the αTAT1 isoforms are comparable in size to YFP–FKBP (for example, 34 kDa for human αTAT1 isoform 4) and are thus expected to enter the MT lumen via diffusion. To test the general effect of molecular size on luminal access, it may be useful to perform a luminal trapping assay and measure the propagation rate of YFP–FKBP fused to a load protein of varying size[35,36].

Besides molecular size, one influential factor on luminal propagation will be the binding affinity for the MT lumen[16,19]. Because the affinity of αTAT1 to MTs is different from that between FKBP and FRB[37], the mechanism of αTAT1 luminal entry cannot be readily inferred from the present result. It would thus be interesting to perform the luminal trapping assay using an inducible dimerization pair with binding affinity similar to that between αTAT1 and tubulins[38]. It would also be of interest to modify the trapping assay so that it becomes possible to explore a previously proposed mechanism of αTAT1 entry, whereby αTAT1 scans the outer surface of MTs and looks for apertures to gain direct access into the lumen[7,39].

Through our studies, we have also confirmed the importance of characterizing MT properties in a comprehensive manner. Based on the type of sample preparation, MTs could exhibit distinct features (for example, molecular constituents, post-translational modifications and structural integrity). These differences could impact the biophysical characteristics of the MTs, including luminal accessibility. Testing out different MT preparations along with careful data interpretation would be ideal.

In view of its modular design principle, we foresee potential of our inducible trapping approach for three feasible applications. First, it would be exciting to examine whether specialized intracellular MT organization (such as cilia axonemes and spindle bodies) will retain luminal accessibility comparable to that of cytosolic MTs. Second, the MT inner proteins (MIPs) identified in *Chlamydomonas reinhardtii*[40], and their human orthologs, may offer a new series of FRB diffusion traps. Third, with chemically inducible recruitment of tubulin acetyltransferases or deacetylases as FKBP fusions[12,13,41], we may be able to achieve rapid modification of the acetylation status of MTs, which would help examine the role of tubulin acetylation on MT mechanics and biology. In conclusion, the trapping assay developed in the present study as well as the insights derived from its implementation may facilitate future exploration of the MT lumen as a driver of cellular functions.

Online content

Any methods, additional references, Nature Research reporting summaries, source data, extended data, supplementary information, acknowledgements, peer review information; details of author contributions and competing interests; and statements of data and code availability are available at https://doi.org/10.1038/s41589-021-00791-w.

Received: 25 July 2020; Accepted: 30 March 2021;
Published online: 3 May 2021

References

1. Janke, C. & Magiera, M. M. The tubulin code and its role in controlling microtubule properties and functions. *Nat. Rev. Mol. Cell Biol.* **21**, 307–326 (2020).
2. Goodson, H. V. & Jonasson, E. M. Microtubules and microtubule-associated proteins. *Cold Spring Harb. Perspect. Biol.* **10**, a022608 (2018).
3. Bodakuntla, S., Jijumon, A. S., Villablanca, C., Gonzalez-Billault, C. & Janke, C. Microtubule-associated proteins: structuring the cytoskeleton. *Trends Cell Biol.* **29**, 804–819 (2019).
4. Garvalov, B. K. et al. Luminal particles within cellular microtubules. *J. Cell Biol.* **174**, 759–765 (2006).
5. Burton, P. R. Luminal material in microtubules of frog olfactory axons: structure and distribution. *J. Cell Biol.* **99**, 520–528 (1984).
6. Peters, A., Proskauer, C. C. & Kaiserman-Abramof, I. R. The small pyramidal neuron of the rat cerebral cortex. *J. Cell Biol.* **39**, 604–619 (1968).
7. Janke, C. & Montagnac, G. Causes and consequences of microtubule acetylation. *Curr. Biol.* **27**, R1287–R1292 (2017).
8. Xu, Z. et al. Microtubules acquire resistance from mechanical breakage through intralumenal acetylation. *Science* **356**, 328–332 (2017).
9. Portran, D., Schaedel, L., Xu, Z., Théry, M. & Nachury, M. V. Tubulin acetylation protects long-lived microtubules against mechanical ageing. *Nat. Cell Biol.* **19**, 391–398 (2017).
10. Shah, N. et al. TAK1 activation of αTAT1 and microtubule hyperacetylation control AKT signaling and cell growth. *Nat. Commun.* **9**, 1696 (2018).
11. Montagnac, G. et al. αTAT1 catalyses microtubule acetylation at clathrin-coated pits. *Nature* **502**, 567–570 (2013).
12. Akella, J. S. et al. MEC-17 is an α-tubulin acetyltransferase. *Nature* **467**, 218–222 (2010).
13. Shida, T., Cueva, J. G., Xu, Z., Goodman, M. B. & Nachury, M. V. The major α-tubulin K40 acetyltransferase TAT1 promotes rapid ciliogenesis and efficient mechanosensation. *Proc. Natl Acad. Sci. USA* **107**, 21517–21522 (2010).
14. Perdiz, D., Mackeh, R., Poüs, C. & Baillet, A. The ins and outs of tubulin acetylation: more than just a post-translational modification? *Cell. Signal.* **23**, 763–771 (2011).
15. Szyk, A. et al. Molecular basis for age-dependent microtubule acetylation by tubulin acetyltransferase. *Cell* **157**, 1405–1415 (2014).
16. Coombes, C. et al. Mechanism of microtubule lumen entry for the α-tubulin acetyltransferase enzyme αTAT1. *Proc. Natl Acad. Sci. USA* **113**, E7176–E7184 (2016).
17. Ly, N. et al. TAT1 controls longitudinal spreading of acetylation marks from open microtubules extremities. *Sci. Rep.* **6**, 35624 (2016).
18. Soppina, V., Herbstman, J. F., Skiniotis, G. & Verhey, K. J. Luminal localization of α-tubulin K40 acetylation by cryo-EM analysis of fab-labeled microtubules. *PLoS ONE* **7**, e48204 (2012).
19. Odde, D. Diffusion inside microtubules. *Eur. Biophys. J.* **27**, 514–520 (1998).
20. Reid, T. A., Coombes, C. & Gardner, M. K. Manipulation and quantification of microtubule lattice integrity. *Biol. Open* **6**, 1245–1256 (2017).
21. Arnal, I. & Wade, R. H. How does taxol stabilize microtubules? *Curr. Biol.* **5**, 900–908 (1995).
22. Schaap, I. A. T., De Pablo, P. J. & Schmidt, C. F. Resolving the molecular structure of microtubules under physiological conditions with scanning force microscopy. *Eur. Biophys. J.* **33**, 462–467 (2004).
23. Atherton, J., Stouffer, M., Francis, F. & Moores, C. A. Microtubule architecture in vitro and in cells revealed by cryo-electron tomography. *Acta Crystallogr. D Struct. Biol.* **74**, 572–584 (2018).
24. DeRose, R., Miyamoto, T. & Inoue, T. Manipulating signaling at will: chemically-inducible dimerization (CID) techniques resolve problems in cell biology. *Pflug. Arch.* **465**, 409–417 (2013).
25. Lin, Y. C., Phua, S. C., Lin, B. & Inoue, T. Visualizing molecular diffusion through passive permeability barriers in cells: conventional and novel approaches. *Curr. Opin. Chem. Biol.* **17**, 663–671 (2013).
26. Alushin, G. M. et al. High-resolution microtubule structures reveal the structural transitions in αβ-tubulin upon GTP hydrolysis. *Cell* **157**, 1117–1129 (2014).
27. Dunn, K. W., Kamocka, M. M. & McDonald, J. H. A practical guide to evaluating colocalization in biological microscopy. *Am. J. Physiol. Cell Physiol.* **300**, 723–742 (2011).
28. Dráberová, E., Viklický, V. & Dráber, P. Exposure of lumenal microtubule sites after mild fixation. *Eur. J. Cell Biol.* **79**, 982–985 (2000).
29. Dráber, P. et al. Differences in the exposure of C- and N-terminal tubulin domains in cytoplasmic microtubules detected with domain-specific monoclonal antibodies. *J. Cell Sci.* **92**, 519–528 (1989).
30. Ghossoub, R. et al. Septins 2, 7 and 9 and MAP4 colocalize along the axoneme in the primary cilium and control ciliary length. *J. Cell Sci.* **126**, 2583–2594 (2013).
31. Hoebeke, J., Van Nijen, G. & De Brabander, M. Interaction of oncodazole (R 17934), a new anti-tumoral drug, with rat brain tubulin. *Biochem. Biophys. Res. Commun.* **69**, 319–324 (1976).
32. Sáez-Calvo, G. et al. Triazolopyrimidines are microtubule-stabilizing agents that bind the vinca inhibitor site of tubulin. *Cell Chem. Biol.* **24**, 737–750 (2017).
33. Miller, K. E., Kim, Y., Huh, W. K. & Park, H. O. Bimolecular fluorescence complementation (BiFC) analysis: advances and recent applications for genome-wide interaction studies. *J. Mol. Biol.* **427**, 2039–2055 (2015).
34. Cuveillier, C. et al. MAP6 is an intraluminal protein that induces neuronal microtubules to coil. *Sci. Adv.* **6**, eaaz4344 (2020).

35. Lin, Y. C. et al. Chemically inducible diffusion trap at cilia reveals molecular sieve-like barrier. *Nat. Chem. Biol.* **9**, 437–443 (2013).
36. Breslow, D. K., Koslover, E. F., Seydel, F., Spakowitz, A. J. & Nachury, M. V. An in vitro assay for entry into cilia reveals unique properties of the soluble diffusion barrier. *J. Cell Biol.* **203**, 129–147 (2013).
37. Banaszynski, L. A., Liu, C. W. & Wandless, T. J. Characterization of the FKBP·rapamycin·FRB ternary complex. *J. Am. Chem. Soc.* **127**, 4715–4721 (2005).
38. Bayle, J. H. et al. Rapamycin analogs with differential binding specificity permit orthogonal control of protein activity. *Chem. Biol.* **13**, 99–107 (2006).
39. Howes, S. C., Alushin, G. M., Shida, T., Nachury, M. V. & Nogales, E. Effects of tubulin acetylation and tubulin acetyltransferase binding on microtubule structure. *Mol. Biol. Cell* **25**, 257–266 (2014).
40. Ma, M. et al. Structure of the decorated ciliary doublet microtubule. *Cell* **179**, 909–922 (2019).
41. Hubbert, C. et al. HDAC6 is a microtubule-associated deacetylase. *Nature* **417**, 455–458 (2002).

Publisher's note Springer Nature remains neutral with regard to jurisdictional claims in published maps and institutional affiliations.

© The Author(s), under exclusive licence to Springer Nature America, Inc. 2021

Methods

Plasmid construction. YFP-inserted β-tubulin constructs were constructed by standard subcloning with restriction enzymes. Complementary DNAs (cDNAs) encoding fragments of β-tubulin were amplified by standard polymerase chain reaction (PCR) with *Nhe*I and *Hin*dIII for N-terminal fragments and *Eco*RI and *Not*I for C-terminal fragments. cDNA encoding EYFP was amplified with *Hin*dIII and *Eco*RI. These fragments were cloned into pcDNA3.1 vector using *Nhe*I and *Not*I. Constructs for luminal protein trap and MT markers were generated by Gibson assembly. The amplified fragments were cloned into FUGW-puro vector digested with *Age*I and *Eco*RI. For the MAP4m construct, a human truncated mutant (amino acids 800–1152) containing proline-rich domains and affinity domains was used. For EB1–mCherry, human full-length EB1 was used. For the bacterial expression YFP–FKBP plasmid, cDNA encoding YFP–FKBP was inserted into pET28a vector by standard Gibson assembly. For the YFP–FKBP plasmid at high expression level, cDNA encoding YFP–FKBP was inserted into pEYFP-C1 vector by standard restriction enzyme subcloning. All plasmids were verified by Sanger sequencing. The primary structures of the inducible protein trap system and biosensors are described in Supplementary Note 1.

Cell culture. U2OS (ATCC) and HEK293T (ATCC) cells were maintained in DMEM (Corning, 10013CV) supplemented with 10% FBS (Sigma-Aldrich, F6178) and 1% pen-strep (Thermo Fisher, 15140163) at 37 °C under 5% CO_2. These cell lines have not been authenticated and have not been tested routinely for mycoplasma contamination.

Lentivirus production. HEK293T cells were seeded at 6×10^6 cells in a 10-cm culture dish (Corning) with 10 ml of DMEM and incubated for 24 h at 37 °C in 5% CO_2. Transfer plasmid, packaging plasmid (psPAX2, Addgene 12260) and envelope plasmid (pMD2.G, Addgene 12259) were transfected using polyethylenimine (Polysciences, 24765-1) following the standard protocol. At 24 h post transfection, the medium was replaced with fresh DMEM. The viral supernatant was collected at 48 and 72 h post transfection and concentrated by a standard polyethylene glycol precipitation protocol.

Immunofluorescence. For screening of YFP-inserted β-tubulins, U2OS cells were seeded at a density of 20,000 cells per well into a poly-D-lysine-coated eight-well glass chamber (Cellvis, C8-1-N). The next day, cells were transfected with plasmids encoding YFP-tagged β-tubulin. The transfection was performed with FuGENE HD (Promega) according to the manufacturer's protocol. At 24 h post transfection, cells were washed with PBS(−) three times and fixed with 4% paraformaldehyde (PFA) in PBS(−) for 10 min at room temperature. Next, cells were washed with PBS(−) three times and permeabilized and blocked with 2% BSA and 0.1% Triton X-100 in PBS(−) for 1 h at room temperature. After blocking, cells were incubated with primary antibody against tubulin (clone YL1/2, Millipore Sigma, MAB1864) diluted in blocking buffer overnight at 4 °C. Cells were then washed with PBS(−) three times and incubated with diluted anti-rat secondary antibody conjugated with Alexa Fluor 647 (Thermo Fisher Scientific, A21247) at 1:10,000 and 0.1 μg ml^{-1} of DAPI in blocking buffer for 1 h at room temperature. Cells were washed with PBS(−) three times again and subjected to fluorescence imaging performed on an Eclipse Ti inverted fluorescence microscope (Nikon) equipped with ×100 oil-immersion objective lens (Nikon) and Zyla 4.2 plus sCMOS camera (Andor).

For immunofluorescence of FRB-fused tubulins, U2OS cells were seeded at a density of 10,000 cells per well into a poly-D-lysine-coated eight-well glass chamber. The next day, cells were transduced with lentivirus expressing FRB-fused β-tubulins. The transduction was performed with serum-free plain DMEM with 6 μg ml^{-1} of polybrene. After 48 h post transduction, fixation with PFA, permeabilization, blocking, primary and secondary antibody treatments were performed as described above. Primary antibody against V5 (Thermo Fisher Scientific, R960-25) was used at 1:1,000 and anti-mouse secondary antibody conjugated with Alexa Fluor 568 (Thermo Fisher Scientific, A11004) was used at 1:10,000. For immunofluorescence with detergent-extracted MTs, transduced cells were washed with MT stabilization buffer (MSB; 80 mM PIPES, 2 mM EGTA, 2 mM $MgCl_2$, 4% PEG8000) and permeabilized with 0.2% Triton X-100 in MSB for 4 min at 37 °C. The cells were then washed with MSB three times and incubated with primary V5 antibody diluted in MSB at 1:1,000. After incubation for 30 min at 37 °C, the cells were washed with MSB three times and fixed with 4% PFA in MSB for 10 min at 37 °C. The cells were washed with MSB three times and incubated with secondary antibody and 0.1 μg ml^{-1} of DAPI in MSB for 1 h at room temperature. After washing cells with MSB three times, the samples were subjected to fluorescence imaging.

For immunofluorescence of translocated YFP–FKBP, U2OS cells expressing the indicated FRB–tubulin constructs were seeded at a density of 10,000 cells per well into a poly-D-lysine-coated eight-well glass chamber. The next day, cells were transduced with lentivirus expressing YFP–FKBP. The transduction was performed with serum-free plain DMEM with 6 μg ml^{-1} of polybrene. At 24 h post transduction, cells were treated with DMSO or nocodazole if indicated, followed by 5-min exposure to 100 nM rapamycin. Next, cells were extracted with 0.2% Triton X-100 in MSB as described above for removing free YFP–FKBP and fixed with 4% PFA in MSB for 10 min at 37 °C. Permeabilization, blocking, primary and secondary antibody treatments were performed as described above. Primary antibodies against GFP (Cell Signaling Technology, 2956), acetylated tubulin (Sigma, T7541, clone 6-11B-1) and α-tubulin (Thermo Fisher Scientific, 62204, clone DM1A) were used at 1:1,000. Anti-rabbit secondary antibodies conjugated with Alexa Fluor 488 (Thermo Fisher Scientific, A21206), Alexa Fluor 514 (Thermo Fisher Scientific, A31558) and anti-mouse secondary antibody conjugated Alexa Fluor 633 (Thermo Fisher Scientific, A21052) were used at 1:10,000.

Live-cell imaging. To generate U2OS cells stably expressing FRB-fused β-tubulins, the U2OS cells were seeded at a density of 100,000 cells per well into six-well plates (Corning). The next day, cells were transduced with lentivirus expressing FRB-fused β-tubulins. The transduction was performed with serum-free plain DMEM with 6 μg ml^{-1} of polybrene and at a multiplicity of infection (MOI) of 0.3. At 48 h post transduction, antibiotic screening was performed using 2 μg ml^{-1} puromycin. The puromycin screening was completed for seven days and the expression of FRB-fused tubulins was confirmed by immunofluorescence against the V5 tag. For live-cell imaging, U2OS cells stably expressing FRB-fused β-tubulins were seeded at a density of 5,000 cells per well into an eight-well poly-D-lysine-coated glass chamber and, next day, the cells were transduced with lentivirus expressing CFP–MAP4m at a MOI of 1. At 24 h post initial transduction, the cells were transduced again with lentivirus expressing YFP–FKBP at a MOI of 1 and incubated for an additional 24 h before performing live-cell imaging. For live imaging with taxol, cells were incubated for 24 h after the second YFP–FKBP transduction and then treated with 1 μM taxol (Sigma-Aldrich, T7402) for 24 h before live-cell imaging. For wide-field fluorescence imaging, an Eclipse Ti inverted fluorescence microscope equipped with a ×60 oil-immersion objective lens and Zyla 4.2 plus sCMOS camera was used. For TIRF imaging, an Eclipse Ti inverted fluorescence microscope equipped with a ×100 oil-immersion TIRF objective lens and pco.edge sCMOS camera (PCO) was used. Time-lapse imaging was conducted at 37 °C, 5% CO_2 and more than 90% humidity using a stage-top incubator (Tokai Hit) at 1-min intervals for 30 min. For induction of the FKBP–FRB interaction, cells were treated with 100 nM rapamycin. For the EB1–mCherry imaging, U2OS cells were seeded at a density of 5,000 cells per well into an eight-well poly-D-lysine-coated glass chamber and, next day, the cells were transduced with lentivirus expressing CFP–MAP4m and EB1–mCherry at MOIs of 1 and 2, respectively. At 48 h post transduction, live-cell imaging was performed with the TIRF microscope. For the EB1–mCherry imaging with nocodazole, cells were prepared as described above and live-cell imaging was performed with a wide-field fluorescence microscope. During the live-cell imaging, cells were treated with 5 μM nocodazole (Sigma-Aldrich, M1404). For the translocation experiment with long-lived MTs, cells were treated with 5–10 μM nocodazole for 15–20 min before the experiment, as indicated. For the nocodazole wash-out experiment, cells expressing FRB-tubulins were seeded and transduced with CFP–MAP4m and YFP–FKBP as described above. Before live-cell imaging under nocodazole (+Noc condition), cells were treated with 10 μM nocodazole for 10 min, followed by 100 nM rapamycin and 10 μM nocodazole treatment for 5 min. The nocodazole was washed out and cells were imaged again after 10-min incubation (Noc wash-out condition).

Protein purification. The YFP–FKBP proteins were expressed in BL21 Codon Plus DE3-RIPL (Agilent Technologies) cultured in LB/Kan/Cam media supplemented with 300 μM IPTG for 20 h at 19 °C. The cells were resuspended with 50 mM Tris-HCl (pH 7.5 at room temperature), 250 mM NaCl, 20 mM imidazole and 7 mM β-mercaptoethanol supplemented with protease inhibitor cocktail (Sigma-Aldrich, 11873580001), and lysed by a microfluidizer. The proteins were purified with Ni-NTA agarose (Qiagen) through stepwise elution with 20, 50 and 100 mM imidazole in 50 mM Tris-HCl, 250 mM NaCl, 7 mM β-mercaptoethanol and dialyzed against 25 mM Tris-HCl, 250 mM NaCl, 7 mM β-mercaptoethanol and 20% glycerol. His-tag was cleaved by adding in-house-made 6xHis-MBP–TEV protease (S219V) at a ratio of 20:1 (6xHis-YFP–FKBP:TEV protease (wt/wt)) and dialyzing overnight against 25 mM Tris (pH 7.5 at room temperature), 150 mM NaCl and 7 mM β-mercaptoethanol. Uncleaved 6xHis-YFP–FKBP and 6xHis-MBP–TEV protease (S219V) were removed by passing through Ni-NTA agarose. YFP–FKBP was then concentrated by an Amicon Ultra-4 10K filter unit (Millipore, UFC801096) and the buffer condition was adjusted to 25 mM Tris, 150 mM NaCl, 7 mM β-mercaptoethanol and 30% glycerol to flash freeze in liquid nitrogen and store at −80 °C.

Extracted cellular MT imaging. For time-lapse imaging of YFP–FKBP translocation into the extracted cellular MTs, U2OS cells stably expressing FRB-fused β-tubulins were seeded at a density of 5,000 cells per well into an eight-well poly-D-lysine-coated glass chamber. Next day, cells were transduced with lentivirus expressing β-tubulin–mCherry for visualizing cellular MTs. At 48 h post transduction, cells were extracted with 0.2% Triton X-100 in MSB at 37 °C to remove cytosolic FRB-fused tubulins. Before cytoplasmic extraction, cells were treated with 5 μM nocodazole for 10 min if indicated. After washing the extracted cells with MSB three times, recombinant YFP–FKBP was added at 1 μM or 5 μM.

Time-lapse TIRF imaging was conducted at 37 °C, 5% CO_2 and more than 90% humidity using a stage-top incubator, at 1-min intervals for 30 min. For induction of the FKBP–FRB interaction, cellular MTs were treated with 10 μM or 50 μM rapamycin.

For fluorescence detection of luminal YFP–FKBP translocation, U2OS cells stably expressing FRB-fused β-tubulins and β-tubulin–mCherry were electroporated with plasmid encoding YFP–FKBP under the CMV promoter. Electroporation was performed with a Nucleofector 2b device (Lonza), and program X-001 and the Cell Line Nucleofector Kit V (Lonza) were used following the manufacturer's protocol. The cells were seeded at a density of 30,000 cells per well into an eight-well poly-D-lysine-coated glass chamber. At 48 h post transfection, cells were treated with 5 μM nocodazole for 10 min and subsequently subjected to 100 nM rapamycin treatment for 3 min. Then cells were extracted with 0.2% Triton X-100 in MSB at 37 °C to remove cytosolic YFP–FKBP. The luminal YFP signal was detected by TIRF imaging as described above.

Image analysis. For the colocalization analysis between YFP-fused tubulin and total tubulin, ROIs were manually drawn for each cell to calculate the Pearson's correlation coefficient between YFP and total tubulin using MetaMorph (Molecular Devices). Each ROI was positioned to include the whole region of each single cell. For the line-scan analysis, MetaMorph was used. For the analysis of translocation kinetics, averaged fluorescence intensities of YFP from three different ROIs in a single cell were used. To measure the translocation on MTs, each ROI was manually drawn to avoid the nucleus and include the dense regions of MTs, determined by CFP–MAP4m visualization. After background subtraction, the averaged intensities of YFP and CFP from each ROI were divided by the intensity from the whole cell normalized to $t=0$, to compensate for photobleaching. The YFP/CFP ratio was then determined and normalized as $[YFP/CFP]_{t=0}$ to 0 and $Max.[YFP/CFP]_{t=0\text{-}30}$ to 1. The average value of the normalized YFP/CFP ratio from three different ROIs was used to determine the kinetics of YFP–FKBP translocation. The half-time of the translocation was calculated by fitting the kinetics to a single exponential function. For the experiment with Tub-FRB_{outer}, the translocation of YFP–FKBP was too rapid to determine the half-time because of the image acquisition interval, and thus we concluded that the half-time of YFP–FKBP with Tub-FRB_{outer} is shorter than 1 min. For quantification of the EB1-positive MT tips at the cell periphery in TIRF imaging, we selected clearly visible CFP-positive MT tips on the edge of cells and counted the EB1–mCherry-positive rate. For the YFP–FKBP colocalization analysis with TIRF imaging, a ROI of about 100 × 100 pixels was manually drawn for each cell to calculate the Pearson's correlation coefficient between YFP–FKBP and CFP–MAP4m using MetaMorph. The ROI was positioned to include CFP-positive MTs in the peripheral region. The value of the correlation coefficient in the ROI was determined at $t=3$ min (immediately before rapamycin treatment) as Rap(−) and $t=4$ min (1 min post rapamycin addition) as Rap(+). For the colocalization analysis in taxol-treated cells, the ROI was manually drawn on a bundled MT structure. The correlation coefficient in the ROI was calculated at $t=3$ min (immediately before rapamycin treatment) as Rap(−) and $t=13$ min (10 min post rapamycin addition) as Rap(+). For the line-scan analysis of translocated YFP–FKBP along the MTs, a 20-pixel ROI was manually drawn on each MT from the tip of each MT at 1 min and 10 min post rapamycin treatment. The YFP intensity along each MT was measured using MetaMorph. For analysis of halting MT polymerization by nocodazole treatment, EB1 foci were manually counted in each cell and shown as the number of EB1 foci per 100 μm^2. To quantify the YFP–FKBP translocation distance from the MT tips, clearly distinguishable single MTs in cells were manually selected. MTs with detectable tip structure and that were at least 6 μm in length from the tip were chosen for quantification. The translocated YFP-positive lengths were manually measured using NIS-Elements (Nikon). For the quantification of lateral entry frequency, we manually selected clearly visualized and isolated MTs in cells expressing Tub-$FRB_{lumen\text{-}ins}$ after 10 min of rapamycin treatment. Specifically, each selected single MT has a clear single filament of at least 7 μm in length. For each cell, at least three MTs were chosen as described above. The number of YFP-positive signals in the middle of these MTs was manually counted and the lateral entry frequency for each cell was calculated by dividing the total lateral entry count by the total length of quantified MTs.

Reproducibility and statistics. In Extended Data Figs. 2 and 8, pairwise comparisons were conducted using a paired two-tailed *t*-test in Microsoft Excel (Microsoft). No sample size estimates were performed, and our sample sizes are consistent with that typically used in live-cell imaging experiments. Regarding sample exclusion in the live-cell experiments in Fig. 3 and Extended Data Fig. 2, to obtain optimal translocation kinetics, cells expressing YFP–FKBP at too high or too low level were excluded from analysis. No randomization was used because the study does not involve allocation into different experimental groups. No blinding was used, as blinding is not relevant to the study because samples were not grouped and randomized. For all experiments in the main figures, at least three individual experiments were performed on different days, and all attempts at replication were successful. For all experiments in the extended data figures, at least two individual experiments were performed on different days and all attempts at replication were successful. For confirmation of YFP–FKBP purification by SDS–PAGE analysis, the gel image was taken from one experiment. The number of performed individual experiments is indicated in each figure legend.

Reporting Summary. Further information on research design is available in the Nature Research Reporting Summary linked to this Article.

Data availability

The datasets generated during this study are available from the corresponding author upon request. Source data are provided with this paper.

Acknowledgements

We thank R. DeRose, A. D. Roy and H. D. Wu for proofreading the manuscript. This work was supported by discretionary funds to T.I. and by the National Institutes of Health (R01GM123130 and R01GM136858 to T.I.). Y.N. was supported by postdoctoral fellowships from the Japan Society for the Promotion of Science and from the Uehara Memorial Foundation. H.T.M. was supported by Postdoctoral Fellowships from the Japan Society for the Promotion of Science.

Author contributions

Y.N. conceived the project. Y.N. designed, performed and analyzed experiments, and wrote the manuscript in consultation with T.I. H.T.M. performed purification of recombinant YFP–FKBP.

Competing interests

The authors declare no competing interests.

Additional information

Extended data is available for this paper at https://doi.org/10.1038/s41589-021-00791-w.

Supplementary information The online version contains supplementary material available at https://doi.org/10.1038/s41589-021-00791-w.

Correspondence and requests for materials should be addressed to Y.N. or T.I.

Peer review information *Nature Chemical Biology* thanks Maxence Nachury and the other, anonymous, reviewer(s) for their contribution to the peer review of this work.

Reprints and permissions information is available at www.nature.com/reprints.

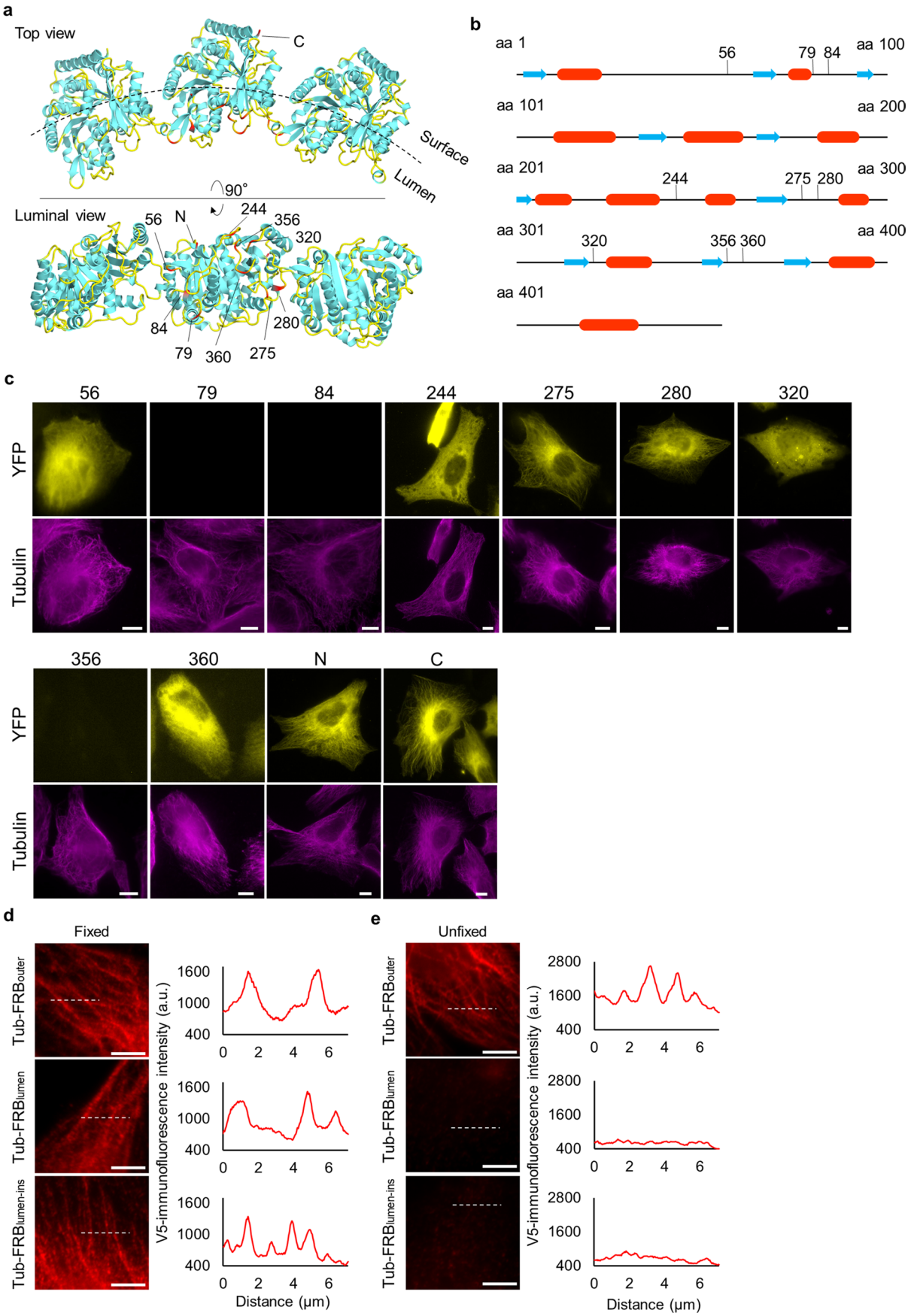

Extended Data Fig. 1 | See next page for caption.

Extended Data Fig. 1 | Characterization of engineered β-tubulin constructs. a, The tested YFP fusion sites in the structure of β-tubulin assembled in a polymerized microtubule. β-tubulin and laterally interacting β-tubulins on both sides are depicted. The loop region in the structure is colored in yellow, otherwise in cyan (PDBID: 3j6g). The fusion sites are indicated and highlighted by red in the middle β-tubulin. N, N-terminus; C, C-terminus. **b**, The secondary structure of β-tubulin. The tested insertion sites are indicated. The α-helices and β-sheets are colored in red and blue, respectively. aa, amino acid. **c**, Screening of YFP-inserted β-tubulin. The insertion sites are indicated. U2OS cells transfected with YFP-fused tubulins (yellow) were immunostained for total tubulin (magenta). Scale bar = 10 μm. **d, e**, Linescan intensity profiles of fixed U2OS cells (**d**) and unfixed cellular MTs from cells (**e**) expressing FRB-fused tubulins. The magnified images are from Fig. 2c and line scan profiles of V5-staining are shown in the right. Scale bar = 10 μm.

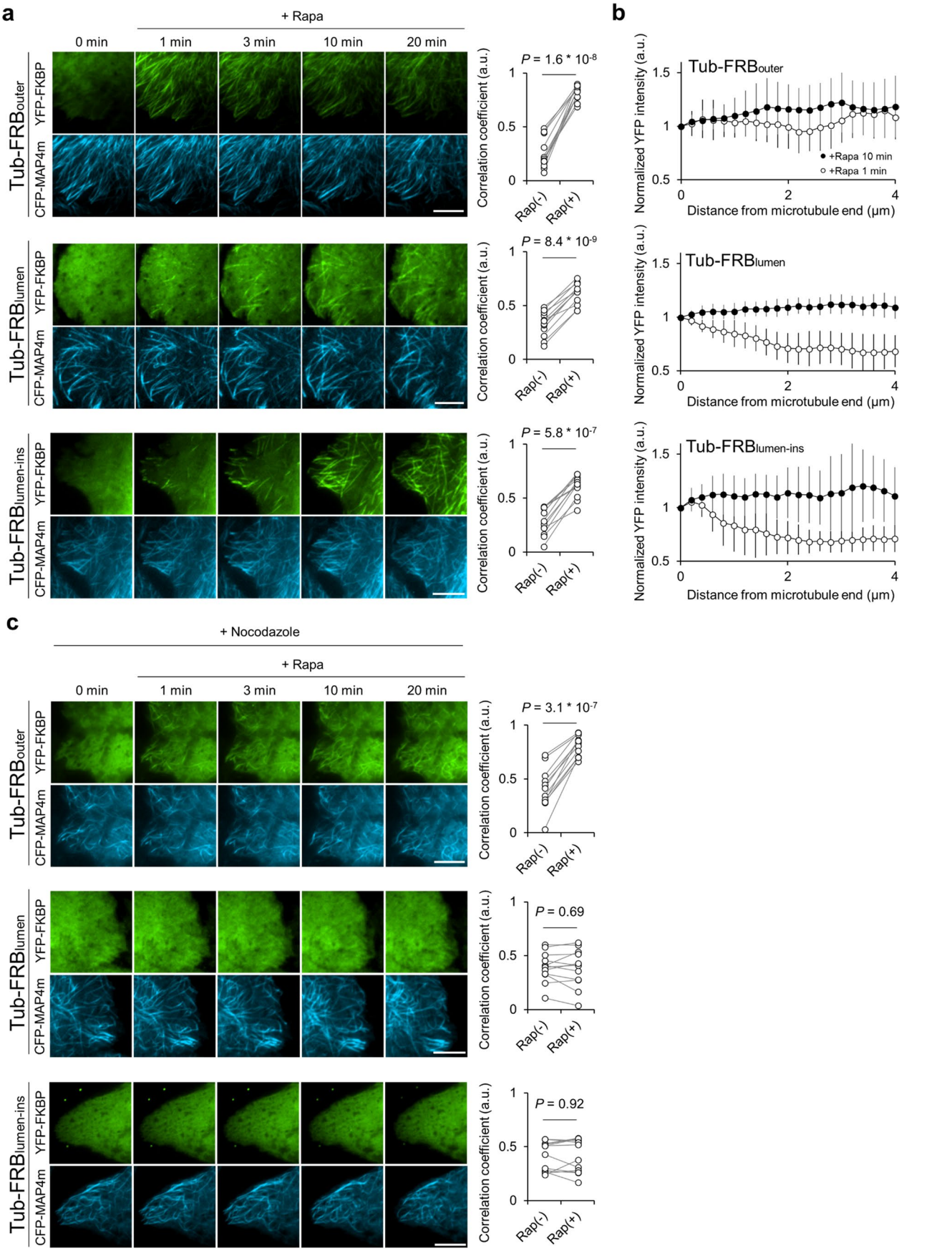

Extended Data Fig. 2 | See next page for caption.

Extended Data Fig. 2 | Cytosolic protein can access the inside of MTs by incorporation into growing MTs. U2OS cells stably expressing FRB-fused tubulins were transduced with YFP-FKBP and CFP-MAP4m. The indicated FRB-fused tubulins were used. Cells were treated with DMSO only (**a**) or 5 μM nocodazole (**c**) for 20 min before time-lapse TIRF imaging, and nocodazole and DMSO treatment were continued during imaging, respectively. The degrees of YFP-FKBP translocation right before (t = 3) and 1 minute after rapamycin treatment (t = 4) were measured by Pearson's correlation coefficient between YFP-FKBP and CFP-MAP4m. Dots are individual data points. Paired two-tailed Student's *t*-tests were performed (n = 12 from three individual experiments). Scale bar = 10 μm. (**b**) Average fluorescence intensity distribution of YFP-FKBP along cellular MTs after 1 (white circles) and 10 min (black circles) incubation with 100 nM rapamycin in **a**. Microtubule tip is located at x = 0 μm. The fluorescence intensity is normalized to the intensity at the tip. Data is shown as mean ± s.d. (n = 10 cellular MTs).

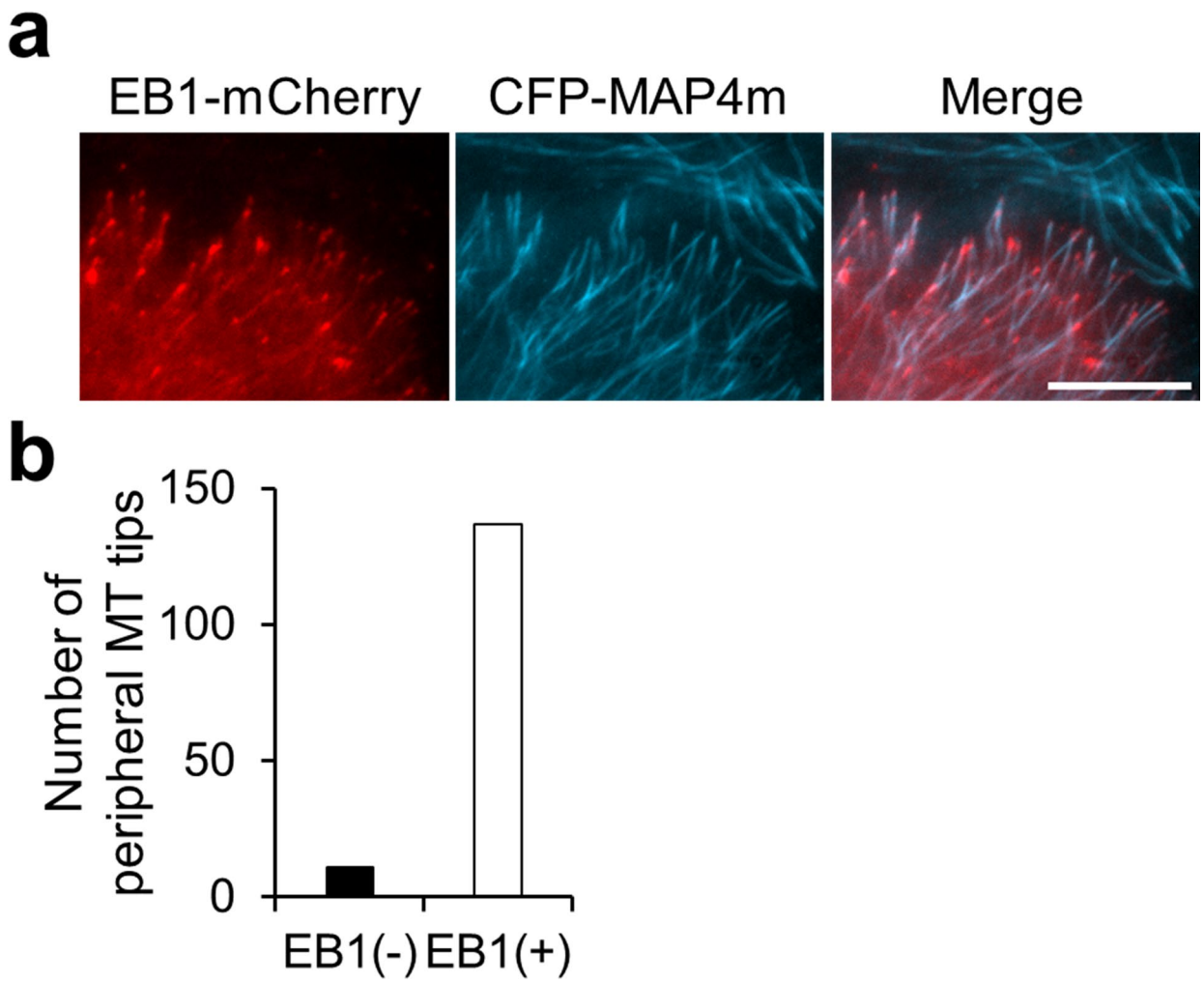

Extended Data Fig. 3 | Microtubule tips located at the periphery of U2OS cells are mainly EB1 positive. a, TIRF imaging of live U2OS cells expressing EB1-mCherry (red) and CFP-MAP4m (cyan). Representative images from two individual experiments are shown. Scale bar = 10 μm. **b**, Quantification of EB1-positive peripheral MT tips in (**a**) (n = 148 peripheral MT tips from 11 cells).

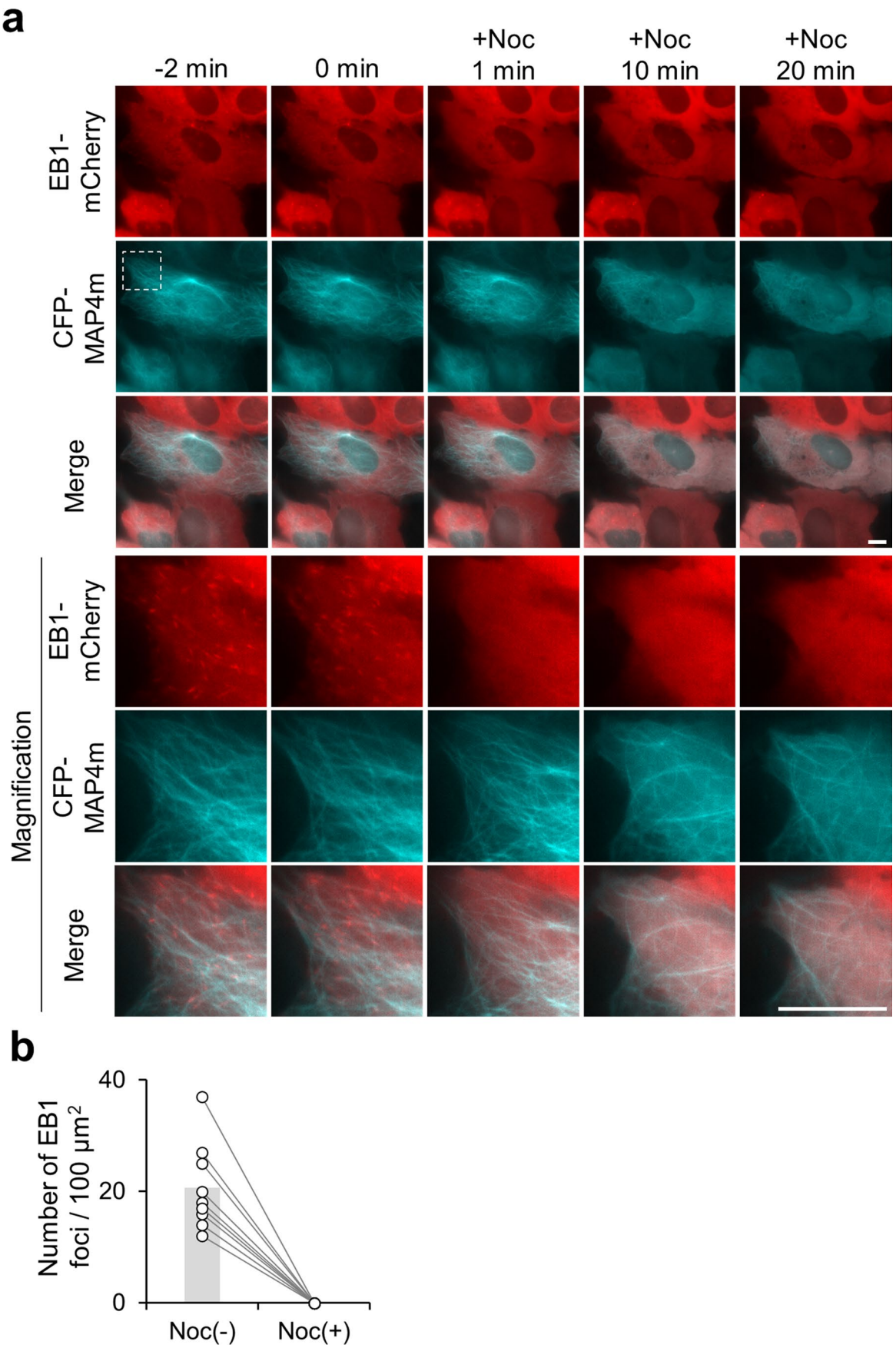

Extended Data Fig. 4 | See next page for caption.

Extended Data Fig. 4 | Nocodazole treatment rapidly halts microtubule polymerization in living cells. a, U2OS cells expressing EB1-mCherry and CFP-MAP4m were treated with 5 μM nocodazole. Magnified images within white square regions are also shown. After 1 min post nocodazole treatment, EB1 foci, indicating the sites of active microtubule polymerization, disappeared. The images are representative from two independent experiments. Scale bar = 10 μm. **b**, Quantification of the number of EB1 foci pre and post nocodazole treatment in **a**. Dots represent individual data points. Bar graph shows mean (n = 9 cells).

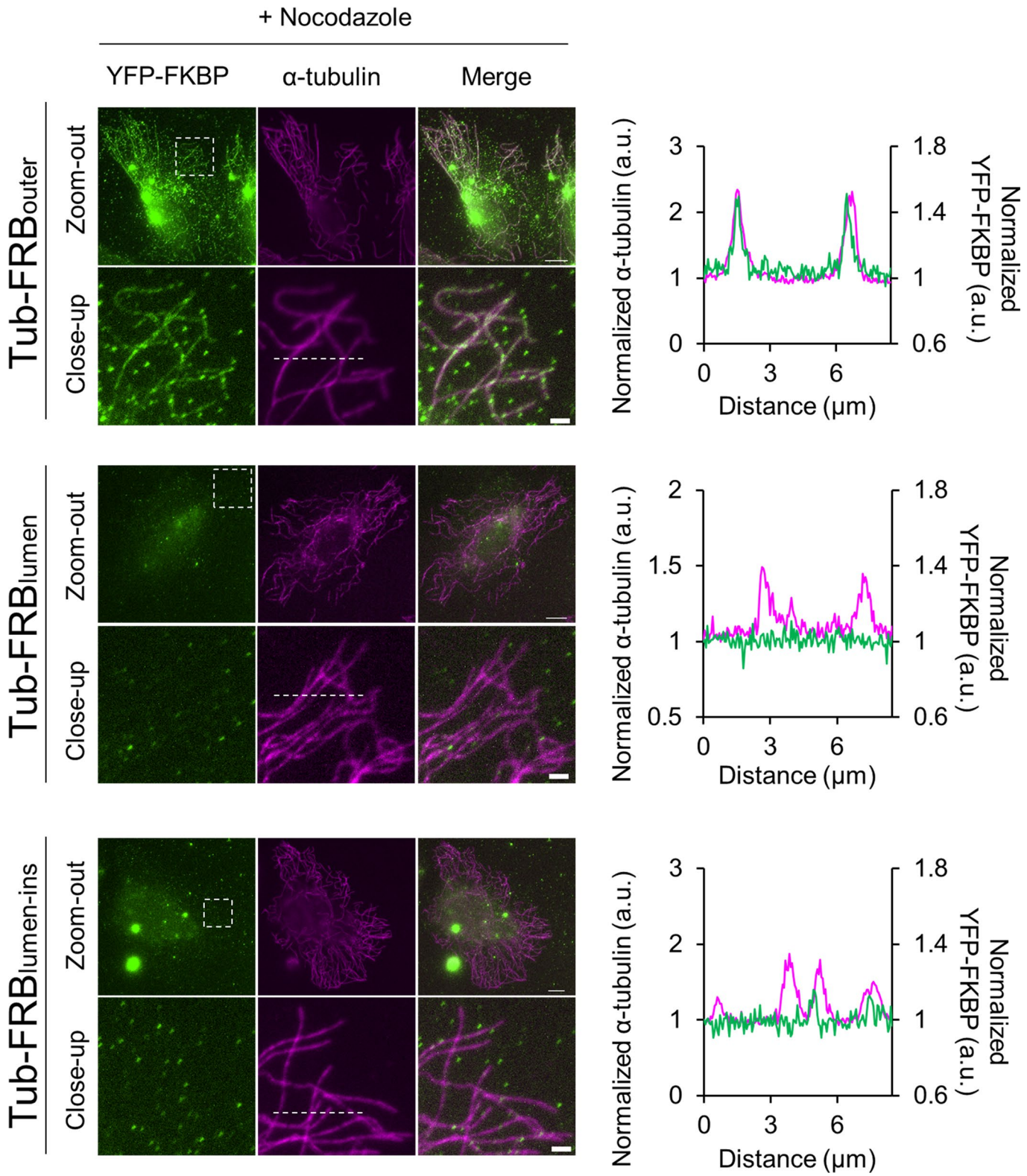

Extended Data Fig. 5 | Immunofluorescence of translocated YFP-FKBP in nocodazole-treated cells with cytosolic extraction. Translocation of YFP-FKBP in U2OS cells stably expressing FRB-fused tubulins treated with 10 μM Nocodazole for 5 min before rapamycin treatment. After 5 min exposure to 100 nM rapamycin, cells were extracted to remove free YFP-FKBP and processed for immunofluorescence against YFP (green) and alpha tubulin (magenta). Indicated FRB-fused tubulins were expressed. Line scan intensity profiles of YFP-FKBP (green) and alpha tubulin (magenta) in the magnified image are also shown. The intensity is normalized to that at 0 μm. Representative images and analyses from two individual experiments are shown. Scale bar = 10 μm (Zoom-out) and 2 μm (Close-up), respectively.

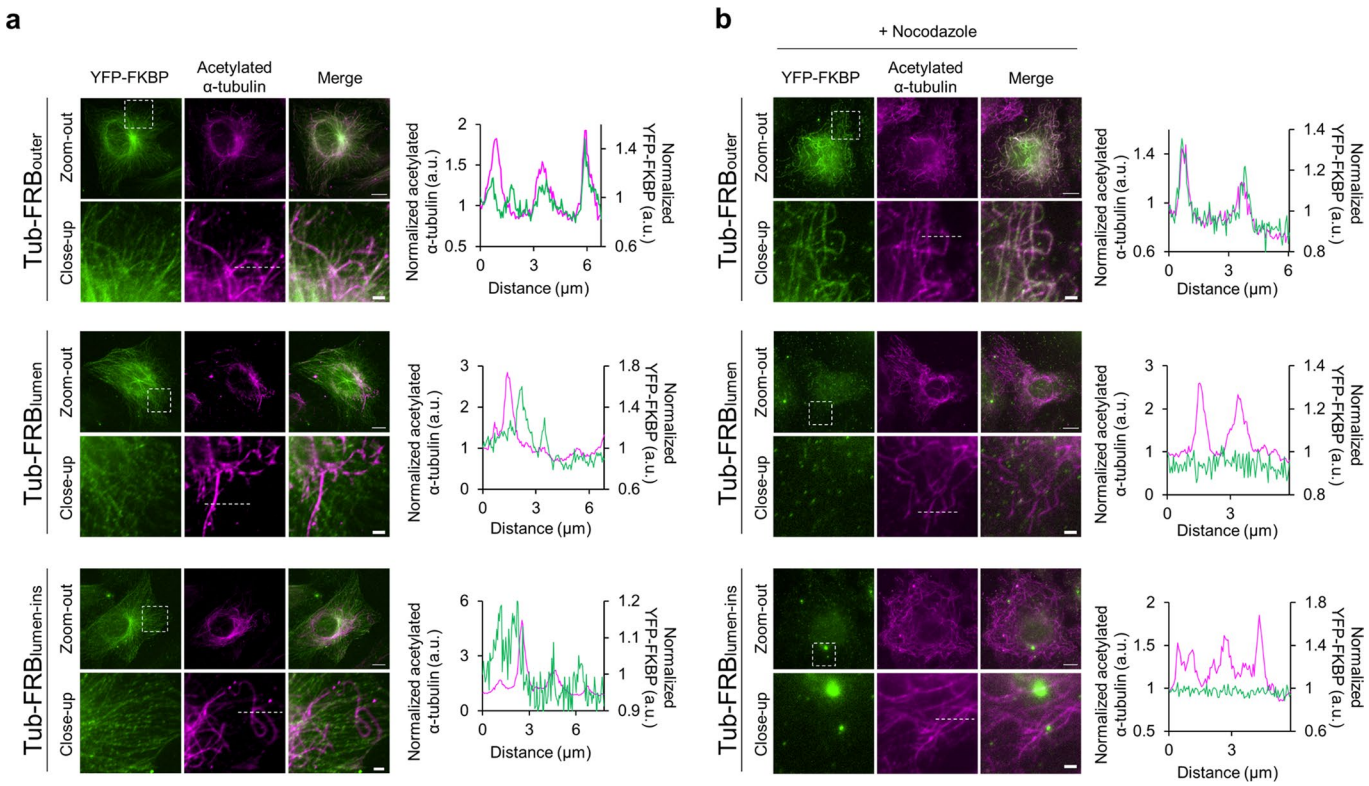

Extended Data Fig. 6 | Luminal incorporation of YFP-FKBP into dynamic MTs. Translocation of YFP-FKBP in U2OS cells stably expressing FRB-fused tubulins treated with vehicle (**a**) or 10 μM Nocodazole for 5 min (**b**) before rapamycin treatment. After 5 min exposure to 100 nM rapamycin, cells were extracted to remove free YFP-FKBP and processed for immunofluorescence against YFP (green) and acetylated tubulin (magenta). Indicated FRB-fused tubulins were expressed. Magnified images within white square region are shown. Line scan intensity profiles of YFP-FKBP (green) and acetylated tubulin (magenta) in the close-up view are also shown. The intensity is normalized to that at 0 μm. Representative images and analyses from two individual experiments are shown. Scale bar = 10 μm (Zoom-out) and 2 μm (Close-up), respectively.

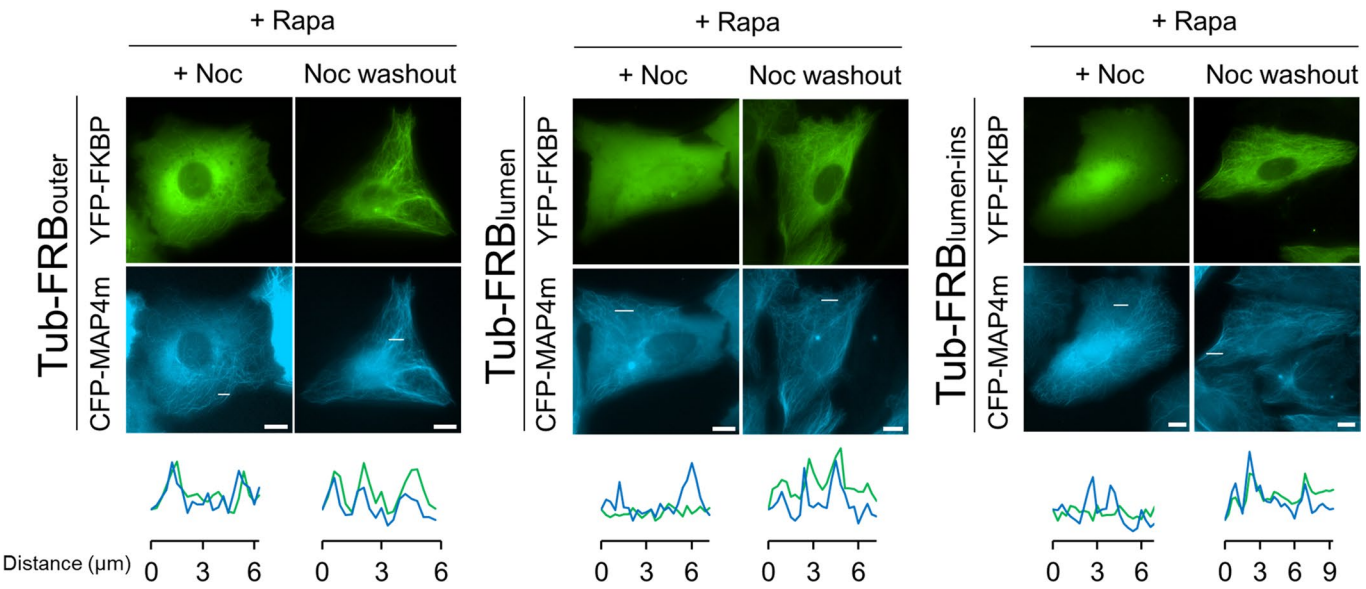

Extended Data Fig. 7 | Tubulin-FRB dimerized with YFP-FKBP is incorporated into microtubules after nocodazole wash-out. Translocation of YFP-FKBP in U2OS cells stably expressing FRB-fused tubulins treated with 10 μM nocodazole for 10 min, followed by 100 nM rapamycin for 5 min (+ Noc). Then nocodazole was washed out and the cells were imaged after 10 min incubation (Noc washout). Indicated FRB-fused tubulins were expressed. CFP-MAP4m was also co-transduced to visualize MTs. Rapa, 100 nM rapamycin. Representative images from two individual experiments are shown. Representative line scan intensity profiles of YFP-FKBP (green) and CFP-MAP4m (blue) in the magnified image are also shown. The intensity is normalized to that at 0 μm. Scale bar = 10 μm.

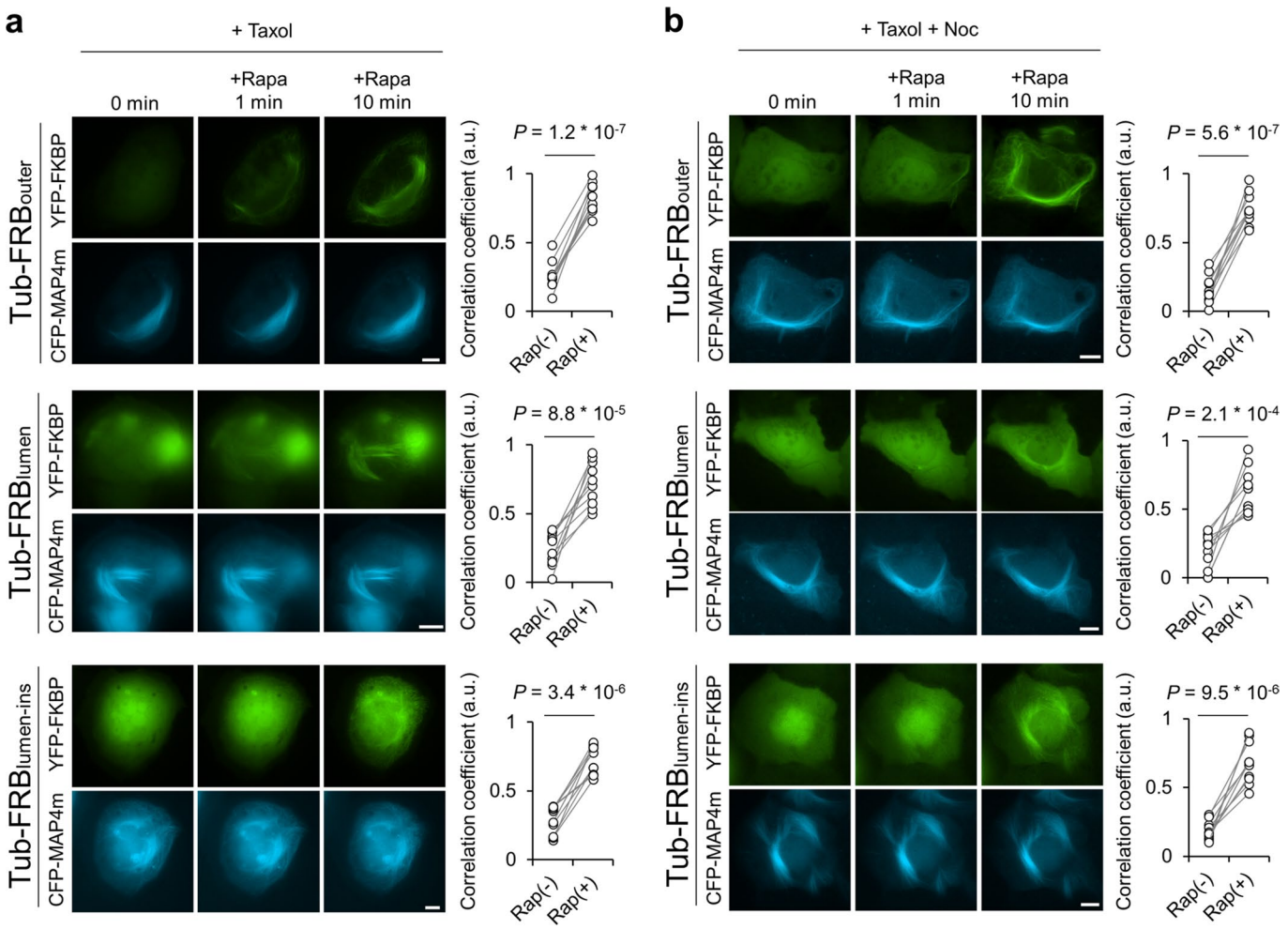

Extended Data Fig. 8 | Soluble proteins can access the lumen of taxol-stabilized cellular MTs. a, Translocation of YFP-FKBP in U2OS cells stably expressing FRB-fused tubulins treated with 1 μM taxol for 24 hr before live cell imaging. Indicated FRB-fused tubulins were expressed. CFP-MAP4m was also co-transduced to visualize MTs. Rapa, 100 nM rapamycin. **b**, The taxol-treated cells were subsequently subjected to 10 μM Nocodazole for 15 min before live cell imaging. The degree of YFP-FKBP translocation was quantified by Pearson's correlation coefficient between YFP-FKBP and CFP-MAP4m. Dots are individual data points. Paired two-tailed Student's *t*-tests were performed (n = 10 from two individual experiments). Scale bar = 10 μm.

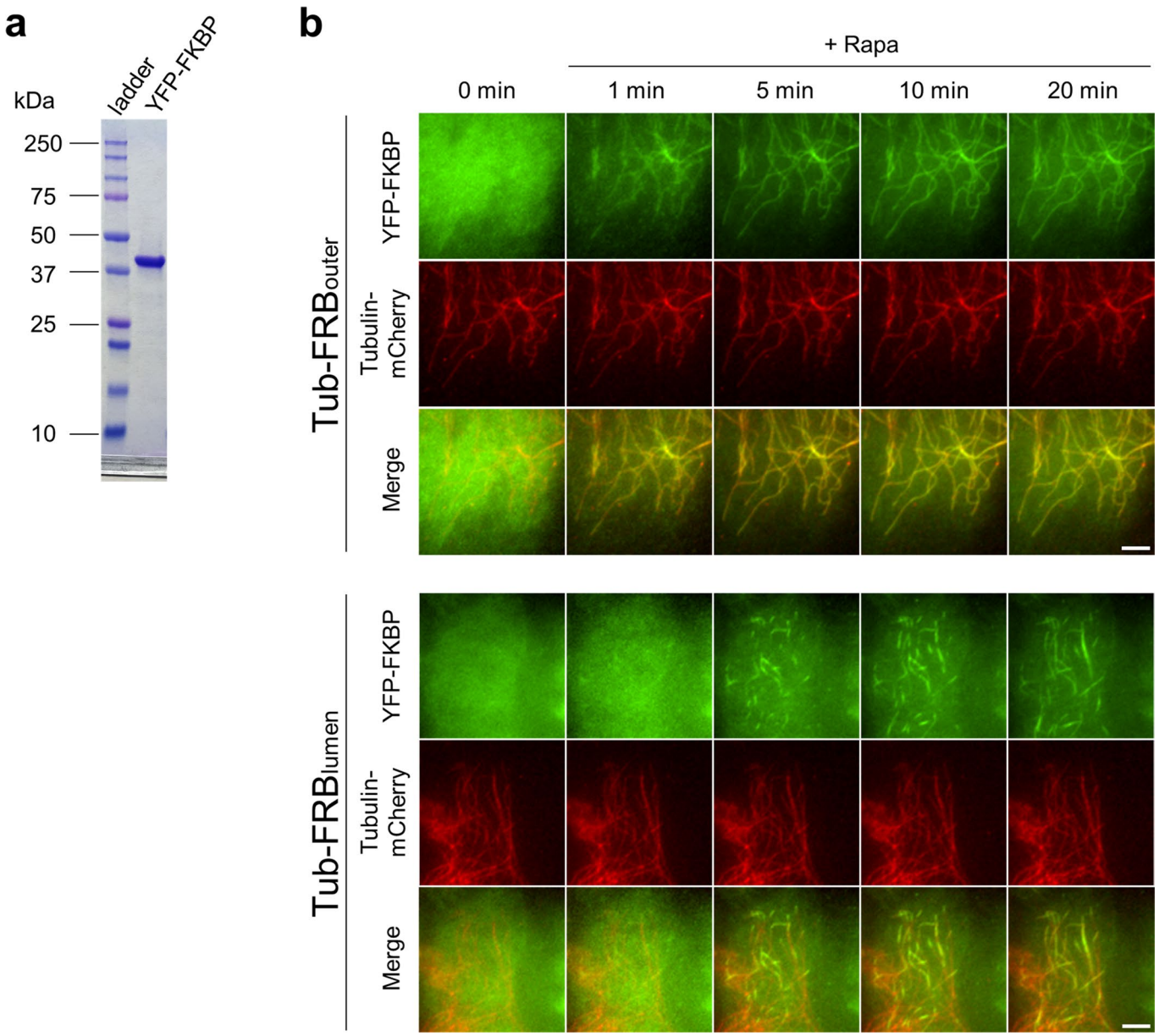

Extended Data Fig. 9 | Luminal trapping assay with extracted cellular MTs. a, An SDS-PAGE gel image of purified YFP-FKBP stained with Coomassie blue. The image is shown from one experiment. **b**, Time lapse TIRF microscopy images from the luminal trapping assay with purified YFP-FKBP using Tub-FRB_{outer} (top) and Tub-FRB_{lumen} (bottom). Scale bar = 5 μm. Representative images are shown from three individual experiments.

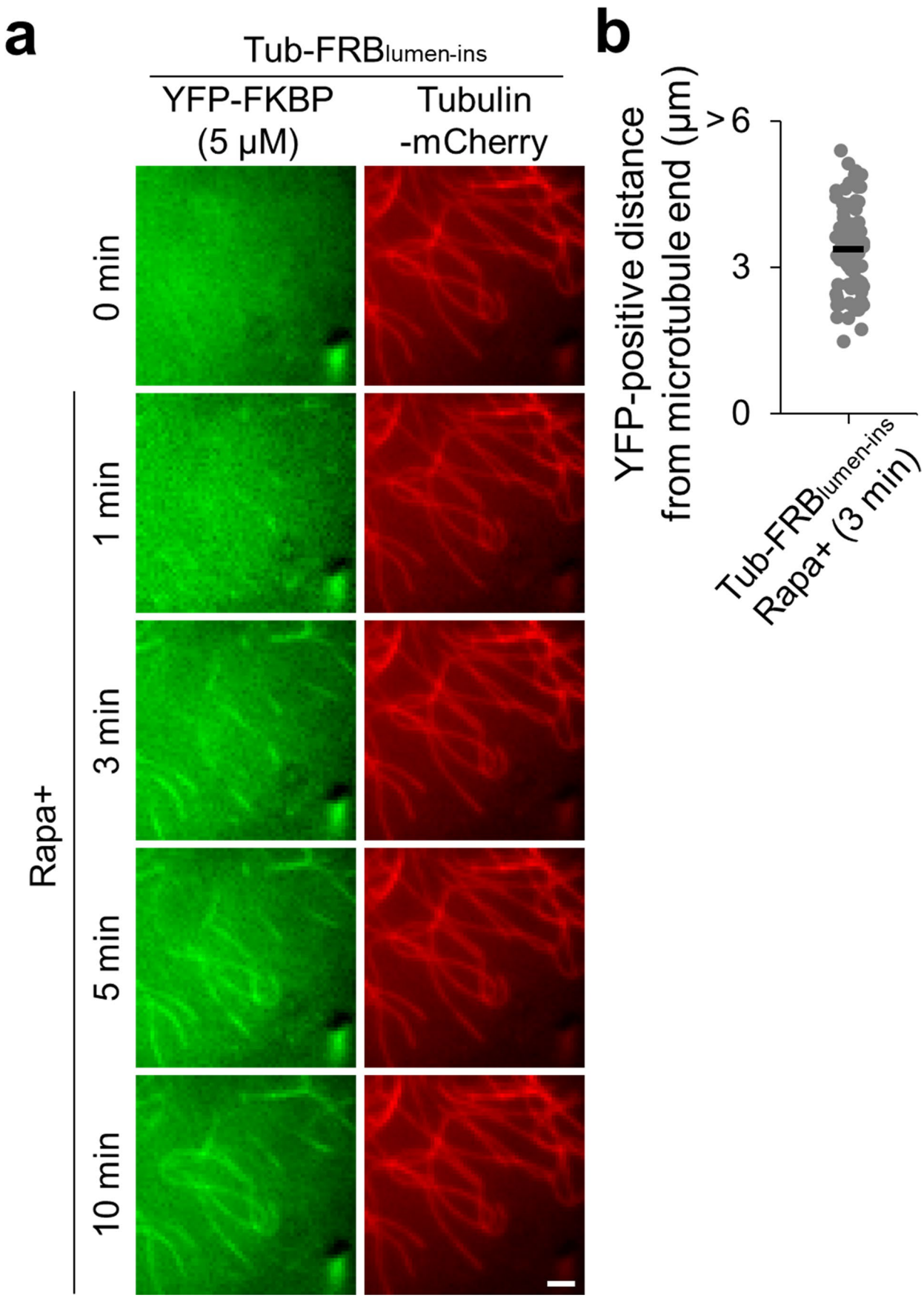

Extended Data Fig. 10 | See next page for caption.

Extended Data Fig. 10 | Kinetics of luminal trapping depends on the concentration of YFP-FKBP probes. a, Representative time lapse TIRF microscopy images of luminal trapping assay with Tub-$FRB_{lumen\text{-}ins}$ and 5 μM of recombinant YFP-FKBP. Scale bar = 2 μm. **b**, Quantification of YFP-positive length from microtubule tips at 3 min post rapamycin treatment in **a**. Gray dots indicate individual data points. Black horizontal line shows mean (n = 72 cellular MTs).

nature research

Corresponding author(s): Takanari Inoue, Yuta Nihongaki

Last updated by author(s): Mar 26, 2021

Reporting Summary

Nature Research wishes to improve the reproducibility of the work that we publish. This form provides structure for consistency and transparency in reporting. For further information on Nature Research policies, see our Editorial Policies and the Editorial Policy Checklist.

Statistics

For all statistical analyses, confirm that the following items are present in the figure legend, table legend, main text, or Methods section.

n/a	Confirmed	
☐	☒	The exact sample size (*n*) for each experimental group/condition, given as a discrete number and unit of measurement
☐	☒	A statement on whether measurements were taken from distinct samples or whether the same sample was measured repeatedly
☐	☒	The statistical test(s) used AND whether they are one- or two-sided *Only common tests should be described solely by name; describe more complex techniques in the Methods section.*
☒	☐	A description of all covariates tested
☒	☐	A description of any assumptions or corrections, such as tests of normality and adjustment for multiple comparisons
☐	☒	A full description of the statistical parameters including central tendency (e.g. means) or other basic estimates (e.g. regression coefficient) AND variation (e.g. standard deviation) or associated estimates of uncertainty (e.g. confidence intervals)
☐	☒	For null hypothesis testing, the test statistic (e.g. *F*, *t*, *r*) with confidence intervals, effect sizes, degrees of freedom and *P* value noted *Give P values as exact values whenever suitable.*
☒	☐	For Bayesian analysis, information on the choice of priors and Markov chain Monte Carlo settings
☒	☐	For hierarchical and complex designs, identification of the appropriate level for tests and full reporting of outcomes
☐	☒	Estimates of effect sizes (e.g. Cohen's *d*, Pearson's *r*), indicating how they were calculated

Our web collection on statistics for biologists contains articles on many of the points above.

Software and code

Policy information about availability of computer code

Data collection	NIS Elements (Nikon, version 5.21.02)
Data analysis	Metamorph (Molecular Devices, version 7.8.12.0), NIS Elements (Nikon, version 5.21.02), Microsoft Excel (Microsoft, version 16.0.13801.20240)

For manuscripts utilizing custom algorithms or software that are central to the research but not yet described in published literature, software must be made available to editors and reviewers. We strongly encourage code deposition in a community repository (e.g. GitHub). See the Nature Research guidelines for submitting code & software for further information.

Data

Policy information about availability of data

All manuscripts must include a data availability statement. This statement should provide the following information, where applicable:

- Accession codes, unique identifiers, or web links for publicly available datasets
- A list of figures that have associated raw data
- A description of any restrictions on data availability

The datasets generated during this study are available from the corresponding authors upon request.

Field-specific reporting

Please select the one below that is the best fit for your research. If you are not sure, read the appropriate sections before making your selection.

☒ Life sciences ☐ Behavioural & social sciences ☐ Ecological, evolutionary & environmental sciences

For a reference copy of the document with all sections, see nature.com/documents/nr-reporting-summary-flat.pdf

Life sciences study design

All studies must disclose on these points even when the disclosure is negative.

Sample size	No sample size estimates were performed, and our sample sizes are consistent with that typically used in live-cell imaging experiments. References: doi: 10.1038/nmeth.1428, doi: 10.1038/s41592-020-0913-x
Data exclusions	To obtain optimal translocation kinetics in live cell experiments described in Fig. 3 and Extended Data Fig.2, cells expressing YFP-FKBP at too high or too low level were excluded from analysis.
Replication	For all experiments in main figures, at least three individual experiments were performed on different days and all attempts at replication were successful. For all experiments in Extended Data figures, at least two individual experiments were performed on different days and all attempts at replication were successful. For confirmation of YFP-FKBP purification by SDS-PAGE analysis, the gel image was taken from one experiment. The number of performed individual experiments is indicated in each figure legend.
Randomization	No randomization was used because the study does not involve allocation into different experimental groups.
Blinding	No blinding was used. Blinding was not relevant to the study because samples were not grouped and randomized.

Reporting for specific materials, systems and methods

We require information from authors about some types of materials, experimental systems and methods used in many studies. Here, indicate whether each material, system or method listed is relevant to your study. If you are not sure if a list item applies to your research, read the appropriate section before selecting a response.

Materials & experimental systems

n/a	Involved in the study
☐	☒ Antibodies
☐	☒ Eukaryotic cell lines
☒	☐ Palaeontology and archaeology
☒	☐ Animals and other organisms
☒	☐ Human research participants
☒	☐ Clinical data
☒	☐ Dual use research of concern

Methods

n/a	Involved in the study
☒	☐ ChIP-seq
☒	☐ Flow cytometry
☒	☐ MRI-based neuroimaging

Antibodies

Antibodies used	Anti-Tubulin antibody (Millipore Sigma, MAB1864, clone YL1/2), Anti-rat secondary antibody conjugated with Alexa Fluor 647 (Thermo Fisher Scientific, A21247), Anti-V5 antibody (Thermo Fisher Scientific, R960-25, clone R960-25), Anti-GFP antibody (Cell Signaling Technology, #2956), Anti-acetylated tubulin antibody (Sigma, T7541, clone 6-11B-1), Anti-alpha tubulin antibody (Thermo Fisher Scientific, 62204, clone DM1A) Anti-mouse secondary antibody conjugated with Alexa Fluor 568 (Thermo Fisher Scientific, A11004), Anti-rabbit secondary antibody conjugated with Alexa Fluor 488 (Thermo Fisher Scientific, A21206), Anti-rabbit secondary antibody conjugated with Alexa Fluor 514 (Thermo Fisher Scientific, A31558), Anti-mouse secondary antibody conjugated with Alexa Fluor 633 (Thermo Fisher Scientific, A21052)
Validation	Anti-Tubulin antibody: Routinely evaluated by Western Blot on A431 lysates by manufacturer. Anti-V5 antibody: Specific V5 detection was confirmed by Western Blot and immunofluorescence of mammalian cells by manufacturer. Anti-GFP antibody: Specific overexpressed GFP, YFP and CFP detection was confirmed by Western Blot and immunofluorescence of mammalian cells by manufacturer. Anti-acetylated tubulin antibody: Specific detection was confirmed by Western Blot and immunofluorescence of mammalian cells by manufacturer. Anti-alpha tubulin antibody: Specific detection was confirmed by Western Blot and immunofluorescence of mammalian cells by manufacturer.

Eukaryotic cell lines

Policy information about cell lines

Cell line source(s)	HEK293T and U2OS cells (ATCC)
Authentication	These cell lines have not been authenticated.
Mycoplasma contamination	Beyond initial testing for mycoplasma contamination which was negative, none of the cell lines have been tested routinely for Mycoplasma contamination.
Commonly misidentified lines (See ICLAC register)	Cell lines used in this paper are not listed in the database of cross-contaminated or misidentified cell lines by ICLAC.